

1965

A Formula for Predicting the Angular Distribution of Thick Target Bremsstrahlung

William Wayne Scott
College of William & Mary - Arts & Sciences

Follow this and additional works at: <https://scholarworks.wm.edu/etd>



Part of the [Physics Commons](#)

Recommended Citation

Scott, William Wayne, "A Formula for Predicting the Angular Distribution of Thick Target Bremsstrahlung" (1965). *Dissertations, Theses, and Masters Projects*. William & Mary. Paper 1539624588.
<https://dx.doi.org/doi:10.21220/s2-r7tj-qp16>

This Thesis is brought to you for free and open access by the Theses, Dissertations, & Master Projects at W&M ScholarWorks. It has been accepted for inclusion in Dissertations, Theses, and Masters Projects by an authorized administrator of W&M ScholarWorks. For more information, please contact scholarworks@wm.edu.

**A FORMULA FOR PREDICTING THE
ANGULAR DISTRIBUTION OF THICK TARGET
BREMSSTRAHLUNG**

A Thesis

Presented to

**The Faculty of the Department of Physics
The College of William and Mary in Virginia**

**In Partial Fulfillment
Of the Requirements for the Degree of
Master of Arts**

By

W. Wayne Scott

1965

**A FORMULA FOR PREDICTING THE
ANGULAR DISTRIBUTION OF THICK TARGET
BREMSSTRAHLUNG**

A Thesis

Presented to

**The Faculty of the Department of Physics
The College of William and Mary in Virginia**

**In Partial Fulfillment
Of the Requirements for the Degree of
Master of Arts**

By

W. Wayne Scott

1965

APPROVAL SHEET

This thesis is submitted in partial fulfillment of
the requirements for the degree of
Master of Arts

Wayne Scott
Author

Approved, June 1965

Robert E. Welsh
Robert E. Welsh, Ph. D.

Rolf G. Winter
Rolf G. Winter, Ph. D.

Morton Eckhouse
Morton Eckhouse, Ph. D.

ACKNOWLEDGMENTS

The author wishes to express his appreciation to the National Aeronautics and Space Administration for the opportunity to write this thesis. Special appreciation and gratitude is given to Dr. Robert E. Welsh for his guidance as faculty advisor. Also the author wishes to express gratitude to the Ling-Temco-Vought Research Center for making available preliminary experimental data.

TABLE OF CONTENTS

	Page
ACKNOWLEDGMENT	iii
LIST OF TABLES	vi
LIST OF FIGURES	ix
LIST OF SKETCHES	xi
ABSTRACT	xii
SUMMARY	xiii
INTRODUCTION	2
 CHAPTER	
I. THEORY OF THICK TARGET ANALYSIS	4
II. RADIATION IN THIN TARGETS	8
III. ELECTRON PENETRATION INTO A TARGET	14
Multiple Electron Scattering	14
Electron Backscatter Out of the Target	17
Nonlinear Energy Loss of Electron in the Target	18
Correction for Electron-Electron bremsstrahlung	19
IV. THE BUILD UP AND ABSORPTION OF PHOTONS IN THE TARGET	21
V. THE DERIVATION OF THE THICK TARGET EQUATION	23

	Page
VI. THEORETICAL RESULTS AND COMPARISONS WITH EXPERIMENTAL DATA	31
VII. FIRST APPROXIMATION CORRECTION TO THE THICK TARGET BREMSSTRAHLUNG SPECTRUM	34
VIII. CONCLUDING REMARKS	38
INDEX OF SYMBOLS	40
REFERENCES	44
VITA	45

LIST OF TABLES

Table	Page
I. Angular distribution of multiple scattered electrons in aluminum in which the electron energy is reduced from $T_0 = 0.5$ MeV to a value T	46
II. Angular distribution of multiple scattered electrons in aluminum in which the electron energy is reduced from $T_0 = 1.0$ MeV to a value T	47
III. Angular distribution of multiple scattered electrons in iron in which the electron energy is reduced from $T_0 = 0.5$ MeV to a value T	48
IV. Angular distribution of multiple scattered electrons in iron in which the electron energy is reduced from $T_0 = 1.0$ MeV to a value T	49
V. Stopping power for aluminum	50
VI. Stopping power for iron	51
VII. Attenuation and buildup coefficients for aluminum	52
VIII. Attenuation and buildup coefficients for iron	53
IX. Thick target bremsstrahlung production in aluminum for $T_0 = 0.5$ and $\phi_d = 0$ degrees	54

Table	Page
X. Thick target bremsstrahlung production in aluminum for $T_0 = 0.5$ MeV and $\varphi_d = 15$ degrees	55
XI. Thick target bremsstrahlung production in aluminum for $T_0 = 0.5$ MeV and $\varphi_d = 30$ degrees	56
XII. Thick target bremsstrahlung production in aluminum for $T_0 = 0.5$ MeV and $\varphi_d = 60$ degrees	57
XIII. Thick target bremsstrahlung production in aluminum for $T_0 = 1.0$ MeV and $\varphi_d = 0$ degrees	58
XIV. Thick target bremsstrahlung production in aluminum for $T_0 = 1.0$ MeV and $\varphi_d = 15$ degrees	59
XV. Thick target bremsstrahlung production in aluminum for $T_0 = 1.0$ MeV and $\varphi_d = 20$ degrees	60
XVI. Thick target bremsstrahlung production in aluminum for $T_0 = 1.0$ MeV and $\varphi_d = 30$ degrees	61
XVII. Thick target bremsstrahlung production in aluminum for $T_0 = 1.0$ MeV and $\varphi_d = 60$ degrees	62
XVIII. Thick target bremsstrahlung production in iron for $T_0 = 0.5$ MeV and $\varphi_d = 0$ degrees	63
XIX. Thick target bremsstrahlung production in iron for $T_0 = 0.5$ MeV and $\varphi_d = 15$ degrees	64
XX. Thick target bremsstrahlung production in iron for $T_0 = 0.5$ MeV and $\varphi_d = 30$ degrees	65

Table	Page
XXI. Thick target bremsstrahlung production in iron for $T_0 = 0.5 \text{ MeV}$ and $\varphi_d = 60 \text{ degrees}$	66
XXII. Thick target bremsstrahlung production in iron for $T_0 = 1.0 \text{ MeV}$ and $\varphi_d = 0 \text{ degrees}$	67
XXIII. Thick target bremsstrahlung production in iron for $T_0 = 1.0 \text{ MeV}$ and $\varphi_d = 20 \text{ degrees}$	68
XXIV. Thick target bremsstrahlung production in iron for $T_0 = 1.0 \text{ MeV}$ and $\varphi_d = 30 \text{ degrees}$	69

LIST OF FIGURES

Figure	Page
1. Dependence of thin target bremsstrahlung intensity spectrum on photon energy k and angle θ_0 for an electron kinetic energy = 1.0 MeV	70
2. Angular distribution of multiple scattered electrons in aluminum in which the electron energy is reduced from 1.0 MeV to a value T	71
3. Ratio of backscattered to incident megavolt electrons plotted as a function of target atomic number . . .	72
4. Thick target bremsstrahlung production in aluminum for an incident electron kinetic energy of 0.5 MeV and a detector angle of 0°	73
5. Thick target bremsstrahlung production in iron for an incident electron kinetic energy of 1.0 MeV and a detector angle of 0°	74
6. Thin target differential cross sections for 0.5 MeV bremsstrahlung at photon energies k , and photon angle 15° and 30°	75
7. Thin target differential cross sections for 1.0 MeV bremsstrahlung at photon energies k , and photon angles 15° and 30°	76

8. Comparison of straight through theory (eq. 21) with multiple scattering theory (eq. 19) and experiment (ref. 14) for an aluminum thick target, electron kinetic energy of 0.5 MeV and detector angle of 30° 77

9. A plot of the $\xi(k)$ factor for a 0.5 MeV electron incident on an aluminum target and a detector angle of 15° 78

10. Comparison of corrected multiple scattering theory (eq. 22) with multiple scattering theory (eq. 19) and experiment (ref. 14) for an aluminum thick target, electron kinetic energy of 0.5 MeV and detector angle of 15° 79

LIST OF SKETCHES

Sketch	Page
1. Radiative interaction	8
2. Collision geometry	12
3. Multiple electron scattering	14
4. Multiple scattering array	15
5. Thick target subdivision	23
6. Schematic of electron scattering in a thin target . .	24
7. Schematic of multiple electron scattering in a thick target	25

ABSTRACT

In the theoretical analysis presented herein a formula is developed for approximating the spectral distribution of thick target bremsstrahlung. The approximate consideration is that the thick target spectrum is considered to be the sum of the contributions from a series of thin targets, one behind the other, bombarded by electrons of decreasing energy. Within each thin target the electron is allowed to scatter according to the Goudsmit-Saunderson electron scattering theory and the bremsstrahlung production at each scattering is predicted by the Bethe-Heitler Bremsstrahlung theory. Comparisons are made between results predicted by the approximate formula and experimental data for aluminum and iron thick targets. On the whole the agreement is reasonably good.

SUMMARY

A theoretical analysis which includes multiple electron scattering as described by a random-walk procedure is presented for predicting the spectrum of bremsstrahlung produced at angles relative to a monoenergetic flux of electrons of normal incidence on thick targets. The approximate assumption is made that the spectral and angular distribution of radiation leaving a thick target can be considered as the sum of the contributions from a series of thin targets, one behind the other, bombarded by electrons of continuously decreasing energy and a superposition of several complex processes. These processes are (1) radiation of electrons in thin targets as predicted by the Bethe-Heitler theory; (2) electron penetration into a medium which includes: (a) multiple electron scattering as predicted by Goudsmit-Saunderson theory, (b) electron backscatter out of the target, (c) nonlinear electron energy losses, and (d) electron-electron bremsstrahlung; (3) the absorption and buildup of photons in the target and (4) a first-approximation correction to the thick target spectrum to account for the inaccuracy of the Bethe-Heitler theory. Comparisons are made between the calculated results and experimental data for aluminum and iron targets. On the whole the agreement is reasonably good.

INTRODUCTION

Electrons that exist in the radiation belt (see, for example, ref. 1) surrounding the earth present a radiation hazard to man and equipment in space explorations. This hazard to manned space vehicles from electrons exists primarily in the form of penetrating secondary radiation that is produced by the energy degradation of electrons in the space-vehicle wall. The radiation, designated as bremsstrahlung, results from collisions of the incoming electrons with the charged particles (atoms, nuclei, or electrons) of which the vehicle wall is composed.

A vehicle wall can be treated as a so-called thin target if the incident electron, while traversing the wall, has only one radiative collision, suffers no significant elastic deflection, and loses no appreciable energy by ionization. However, in practice, this is seldom the case. Generally a space vehicle wall will be representative of a thick target, that is, the wall will be of such a thickness that the majority of the incident electrons will lose sufficient energy to be stopped. For this case, the description of the bremsstrahlung field behind the target is a problem of long standing, complicated by multiple electron scattering, electron energy losses, photon absorption, and shower production which prohibits a rigorous solution for the angular distribution of bremsstrahlung from completely stopped electrons.

Previous estimates of the bremsstrahlung spectra from thick targets for electrons with energies of the order of the rest mass-energy (0.511 MeV) have depended upon the theory developed by Kramer (see ref. 2). However, the validity of Kramer's theory is limited in that (a) the theory estimates the photon energy distribution integrated over all directions of the emitted photons and, (b) the theory is nonrelativistic. Estimates have also been made by Wilson (ref. 3), the author (ref. 4), and others but these results are also in the form of an average over the direction of photon emission and no attempt is made to account for multiple electron scattering within the target.

The significance of the theoretical analysis presented is to be two-fold. First, the analysis is intended to provide a basis formula for approximating, with a reasonable degree of accuracy, the spectral distribution of thick target bremsstrahlung. This application is important for shielding studies since experimental data are scarce and there is a need for theoretical data over a wide electron energy and material range. Secondly, the data presented are complementary to thick target bremsstrahlung experiments.

The computational procedure for computing the bremsstrahlung spectra is programmed in the FORTRAN (FORMula TRANslation) IV language for the IBM 7094 electronic data processing system at the Langley Research Center.

CHAPTER I

THEORY OF THICK TARGET ANALYSIS

For a monoenergetic, monodirectional beam of electrons incident on a thick target, a Random-Walk computer program for the analysis of thick target bremsstrahlung has been generated to take into account various aspects of electron penetration and diffusion: angular deflection, energy losses, spatial propagation, and the radiative process at scattering. For charged particles (in this case electrons) the large number of interactions (running into the ten thousands), which an electron may undergo in a thick target, makes it necessary to resort to a sophisticated scheme in which many successive collisions are grouped into a single step of an artificial random walk. The transition probabilities for the random walk are then obtained from pertinent analytical multiple electron scattering distributions governing angular deflections and energy losses.

The random walk scheme must provide, for each step of the random walk, a rule for selecting an energy loss increment, $E_i - E_{i+1}$, a path length $|t_i - t_{i+1}|$, a change of electron direction from $\left\{ \epsilon_\alpha, \psi_\gamma \right\}$ to $\left\{ \epsilon_{\alpha+1}, \psi_{\gamma+1} \right\}$ and a spatial displacement, $|r_i - r_{i+1}|$. A great variety of schemes are possible, which differ with regard to the theoretical input and

the necessary amount of computing time. The rules according to which the random walk is sampled in the work presented herein have been described in some detail in reference 5.

For this analysis a so-called continuous slowing-down approximation is used to select a constant electron energy loss increment $\Delta E = E_i - E_{i+1}$; for example, as previously stated, the thick target can be subdivided into thin targets in which there will occur an electron energy loss ΔE in each. Consider a target whose thickness corresponds to the residual range of a 1 MeV electron (approximately 0.5 gm/cm^2 of aluminum). The arbitrary selection can be made to subdivide the target into 20 thin targets. Each subdivision will thus correspond to an energy loss of 0.05 MeV.

The path length t_i in each thin target is a function of the energy loss increment according to the following relation

$$\left| t_i - t_{i+1} \right| = \int_{E_i}^{E_{i+1}} \frac{dE}{\frac{dE}{dt}} \quad (1)$$

where dE/dt is the energy loss per cm path length in the target. This energy loss mechanism will be discussed in more detail in a later section of this report.

A simplifying assumption is to be made in the case of the spatial displacement, $\left| r_i - r_{i+1} \right|$. Essentially the spatial parameter r is reduced from three dimensions to only one dimension; for example, the spatial position of the electron is considered to

be along the projected path of the initially incident electron at all times and no lateral deflection in position is to be considered at each scattering. This is a reasonable assumption in that the total path length of the electron within the target is itself relatively small in comparison with the distance between the target and detector position. Thus only a change of direction from

$\left\{ \epsilon_{\alpha}, \psi_{\gamma} \right\}$ to $\left\{ \epsilon_{\alpha+1}, \psi_{\gamma+1} \right\}$ is considered to influence the bremsstrahlung spectrum.

The present analysis of the sampling of data differs from the usual random-walk method which consists of sampling many electron trajectories (called case histories), starting each electron with initial energy E_0 and following it until it comes to rest. Along each of the electron trajectories the change in the polar angles, $\left\{ \epsilon_{\alpha}, \psi_{\gamma} \right\}$, at each scattering is chosen by some arbitrary (unweighted) technique and having chosen the polar angles the result is then multiplied by the appropriate scattering probability as predicted by one of the many multiple scattering theories. It is in this particular sense of scoring that the present analysis differs from the usual random walk method. Within each thin target there will be no arbitrariness in the selection of scattering angles other than the arbitrariness in the total number of scatterings that will be allowed within each thin target. In other words, the electron will be forced to assume predetermined or preset directions (different combinations of polar angles) within each thin target and the appropriate probability for the electrons being scattered

at each set of polar angles will be determined by Goudsmit-Saunderson theory.

In summary of the above discussion, it can be said that the electron is presumed to be normally incident on the first of a series of thin targets with energy E_0 . The bremsstrahlung production in the thin target for this particular angle of incidence, electron energy, and detector geometry is then calculated. The electron direction is then changed and the bremsstrahlung production is again determined for the given parameters. The changing of electron direction and the calculation of bremsstrahlung production is continued until all of the predetermined angles have been assumed. The electron is then considered to be entering into the second thin target with an energy of $E_0 - \Delta E$. The above procedure of changing the angles and calculating the bremsstrahlung production is again repeated. The above sequence of events (random-walk steps) is continued until the electron has been brought to rest, that is, the electron energy reduced to zero. The thick target spectrum is then considered to be the sum of the radiation contributions from each thin target.

The complex processes of electron penetration, diffusion and radiation will now be discussed in a more detailed manner prior to deriving a formula for approximating the bremsstrahlung spectrum.

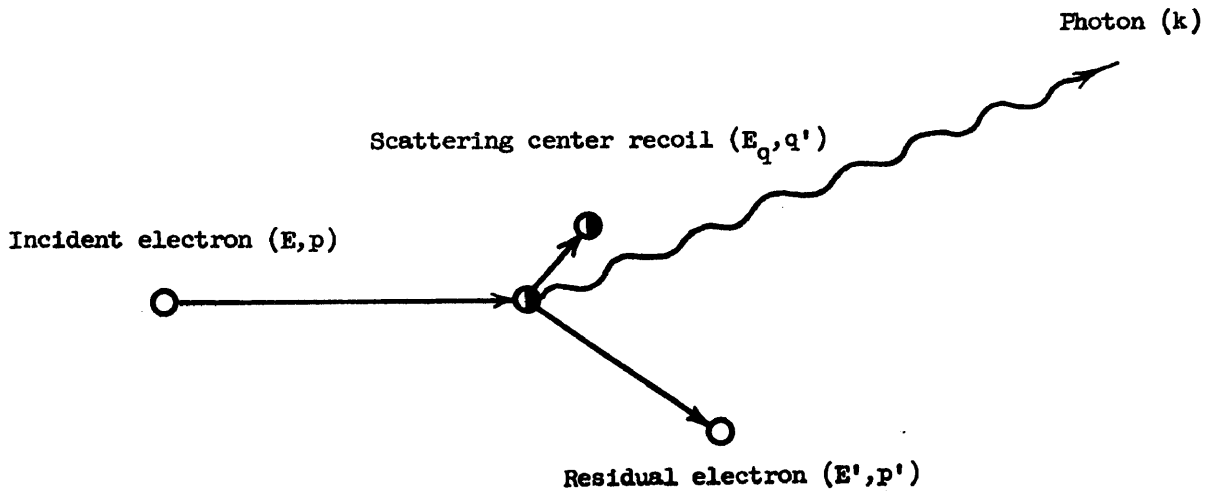
CHAPTER II

RADIATION IN THIN TARGETS

In passing through the field of a nucleus (or atom) an electron with energy E is, in general, deflected. Since this deflection always results in an acceleration, there will be a certain probability that a light quantum (photon) of energy k is emitted with the electron making a transition to another state with residual energy E' , where

$$E = E' + k + E_q \quad (2)$$

This interaction is shown in sketch 1 below.



Sketch 1.— Radiative interaction

In the radiative interaction, shown in sketch 1, the initial momentum of the incident electron becomes shared among three bodies: the residual electron, the scattering center, and the emitted photon. Therefore, the photon can have any momentum and the corresponding energy up to the energy of the incident electron. However, for the radiative interaction of moderate-energy electrons, momentum is substantially conserved between the scattering center and deflected electron, and only a very small amount of momentum is carried away by the photon.

The major part of the quantum-mechanical theory for predicting thin-target bremsstrahlung differential cross-sections has been obtained through the use of the Born approximation technique which is essentially first-order perturbation theory. As a first approximation the atom is considered as stripped, consisting only of the nucleus. This is a good approximation provided

$$\frac{2\pi Ze^2}{h\nu_0} \ll 1 \quad (3)$$

and

$$\frac{2\pi Ze^2}{h\nu} \ll 1 \quad (4)$$

where v_0 , v represent the electron velocity before and after the collision. For light elements equations (3) and (4) are always satisfied if the primary electron moves with relativistic speeds, except in a small frequency range (called high frequency limit)

where the electron has given nearly all its kinetic energy to the light quantum, and after the process, has therefore a small velocity.

The bremsstrahlung cross-section derived for a stripped, infinitely heavy atom using the Born approximation is known as the Bethe-Heitler formula (see ref. 6). This formula can be expressed as a differential with respect to two parameters which are the photon energy k and the solid angle Ω as shown by equation (5). (See eq. (2 BN) of ref. 7.)

$$\begin{aligned}
 d^2 n = \frac{Z^2 r_o^2 p}{8\pi 137 p_o} \frac{dk}{k} d\Omega & \left\{ \frac{8 \sin^2 \theta_o \{2E_o^2 + 1\}}{p_o^2 \Delta_o^4} \right. \\
 & - \frac{2\{5E_o^2 + 2EE_o + 3\}}{p_o^2 \Delta_o^2} - \frac{2\{p_o^2 - k^2\}}{Q^2 \Delta_o^2} + \frac{4E}{p_o^2 \Delta_o} \\
 & + L \left[\frac{4E_o \sin^2 \theta_o \{3k - p_o^2 E\}}{p_o^2 \Delta_o^4} + \frac{4E_o^2 \{E_o + E^2\}}{p_o^2 \Delta_o^2} \right. \\
 & \left. + \frac{2 - 2\{7E_o^2 - 3EE_o + E^2\}}{p_o^2 \Delta_o^2} + \frac{2k\{E_o^2 + EE_o - 1\}}{p_o^2 \Delta_o} \right] \\
 & \left. - \left\{ \frac{4\epsilon}{p\Delta_o} \right\} + \frac{\epsilon^Q}{p^Q} \left[\frac{4}{\Delta_o^2} - \frac{6k}{\Delta_o} - \frac{2k\{p_o^2 - k^2\}}{Q^2 \Delta_o} \right] \right\} \quad (5)
 \end{aligned}$$

where

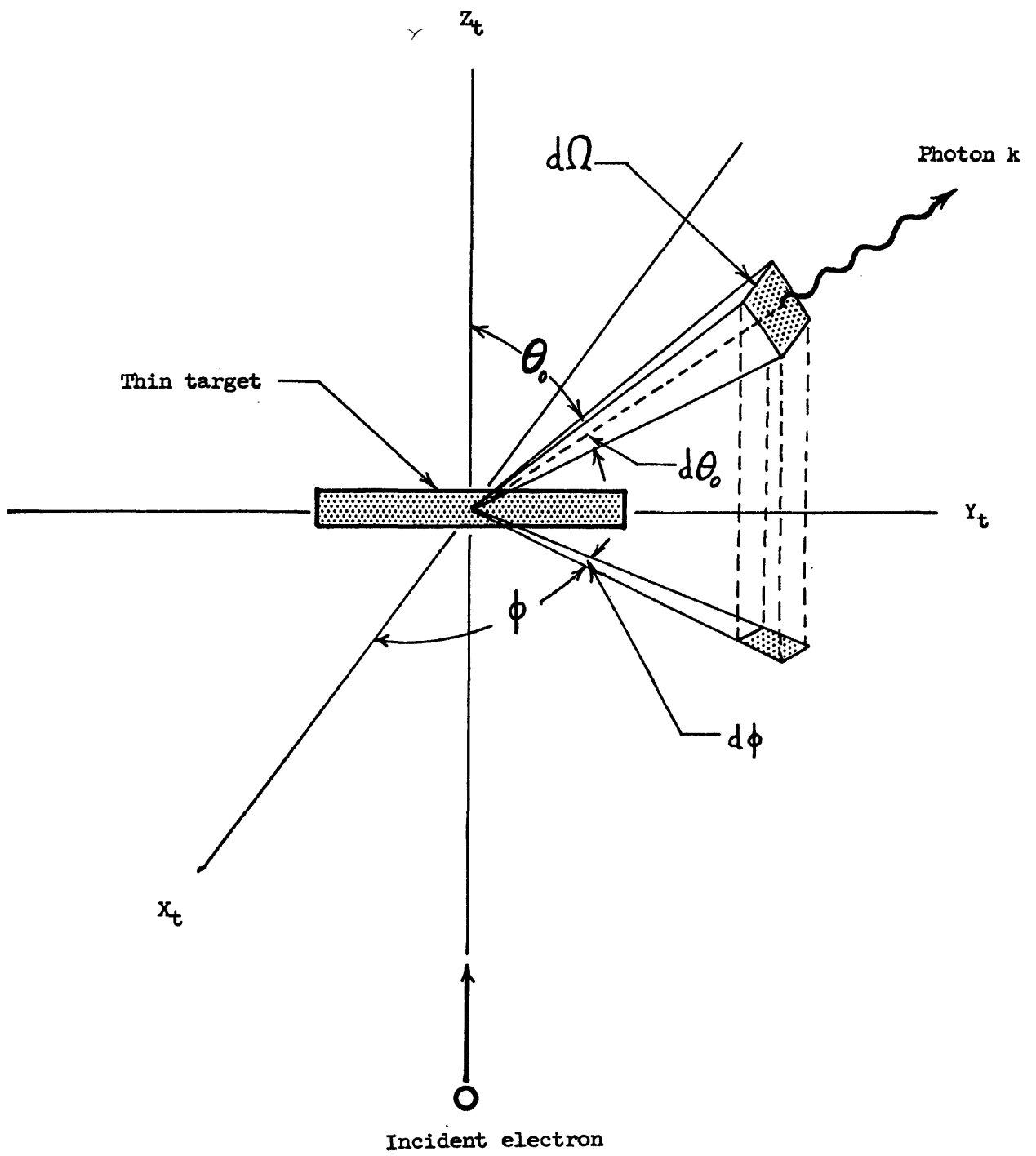
$$L = 2 \ln \left[\frac{EE_0 - 1 + pp_0}{EE_0 - 1 - pp_0} \right], \quad (5a)$$

$$\epsilon_0 = \ln \left[\frac{E_0 + p_0}{E_0 - p_0} \right] \quad (5b)$$

and

$$\epsilon = \ln \left[\frac{E + p}{E - p} \right] \quad (5c)$$

Equation (5) represents the probability that a photon whose energy lies between the limits (k) and $(k + dk)$ shall be emitted within a differential solid angle $(d\Omega)$, oriented (θ_0) with respect to the direction of motion of the incident electron when an electron of total energy E_0 collides with a thin target of atomic number Z . This collision geometry is shown in sketch 2 for an electron approaching the origin along a positive Z_t direction with momentum p_0 and colliding with a thin target which is considered to lie in the x - y plane, perpendicular to the electron direction.



Sketch 2.- Collision geometry

Various corrections are known to exist for the cross-section formula given by equation (5). These corrections may be classified according to three types: (1) coulomb corrections, (2) screening corrections, and (3) high-frequency limit corrections. In each case, the correction is restricted to a particular energy region. This restriction on the energy region is unfortunate because, in the region of interest, roughly 0.1 to 2.0 MeV (intermediate energies), coulomb corrections are not available in analytical form; and empirical corrections cannot be determined in enough detail from the available data to cover the entire energy range. Since screening effects are most important for nonrelativistic or extreme relativistic electron kinetic energies, no screening correction will be made to the cross-section.

The problem of a high-frequency correction, that is, the problem of correcting the cross-section for its apparent error with increasing photon energy, will be dealt with in chapter VII of this report.

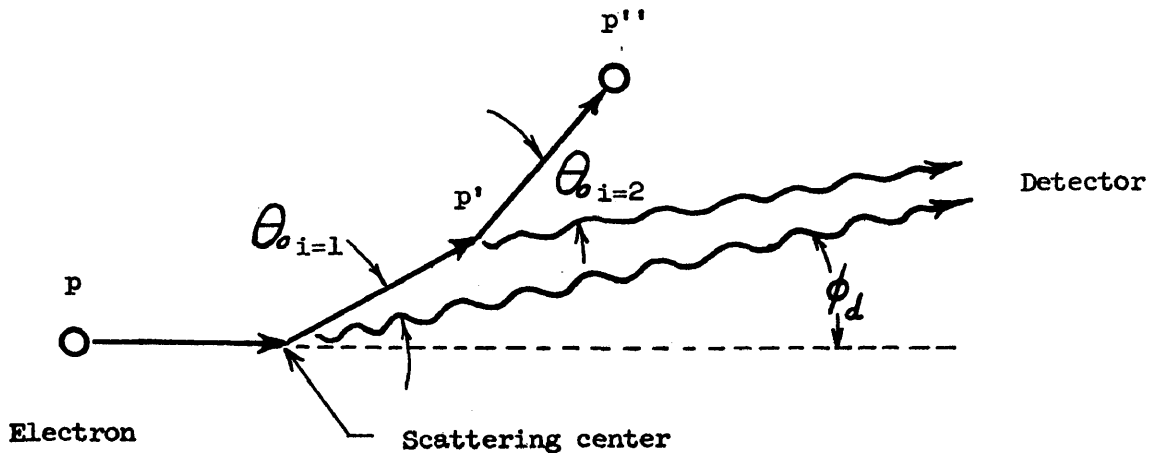
Equation (5) has been evaluated by the author (ref. 4) for a wide range of electron energies and for θ_0 equal to 0° , 30° , 60° , and 90° . One such spectrum from reference 4 is presented in figure 1 for a 1 MeV electron. For convenience the curve has been made independent of the atomic number Z and the cross-section is for a unit, monoenergetic electron flux. It should be noted that the radiation intensity is peaked in the forward direction.

CHAPTER III

ELECTRON PENETRATION INTO A TARGET

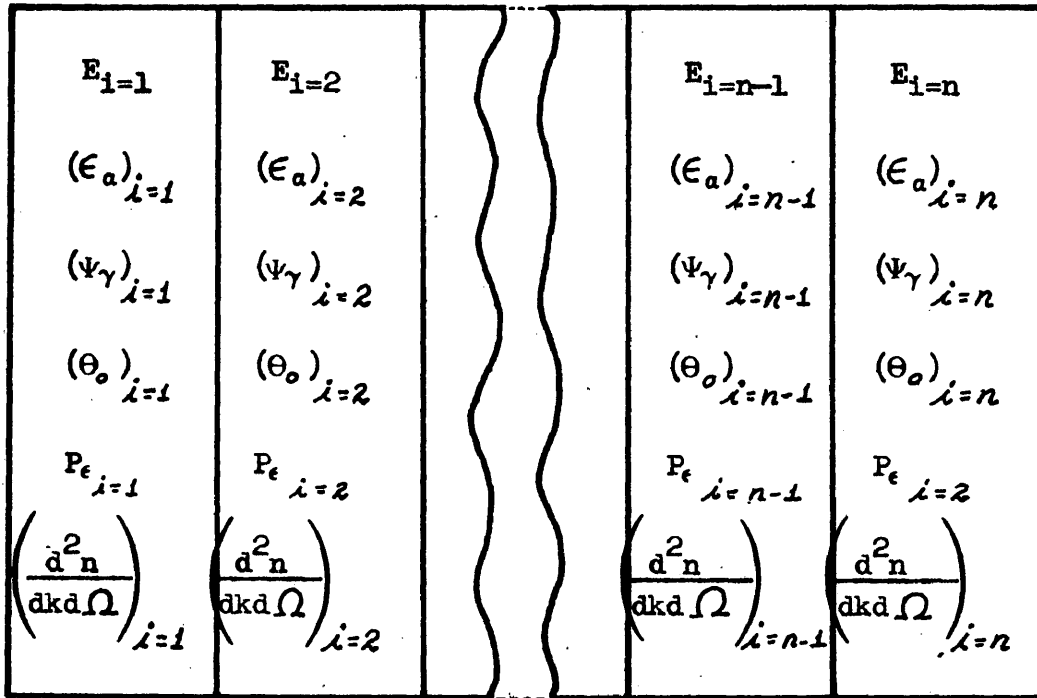
Multiple Electron Scattering

The phenomena of many electron scatterings within a thick absorber are commonly referred to as multiple electron scattering; for example, with each scattering there is an energy loss and a change of direction for the electron. As a consequence of the multiple electron scattering the angular distribution of bremsstrahlung will be altered. This alteration is recognized in that the thin-target bremsstrahlung cross section (eq. (5)) is a function of the angle between the electron direction and the direction of photon emission (detector direction) as shown in sketch 3 below.



Sketch 3.- Multiple electron scattering.

Therefore to include multiple electron scattering in the theoretical analysis the following array within each thin target must be predicted.



Sketch 4.- Multiple scattering array.

In the array of sketch 4 i denotes the particular thin target slab; E_i , the total electron energy in slab i ; ϵ_a, ψ_γ , the polar angles of the electron relative to the incident electron direction; θ_o , the angle between the electron velocity vector and the detector; P_ϵ , the probability of the electron's travelling in the ϵ direction, and $\frac{d^2 n}{dkd\Omega}$, is the cross-section for producing a photon of energy k as a function of E_i, k, θ_o .

The probability, P_ϵ , of the electron's travelling in the ϵ direction can be predicted by one of the many multiple scattering theories, the majority of which are based on the assumption that the scattering process is adequately described by ordinary diffusion. Goudsmit and Saunderson (ref. 8) have derived an expression of multiple

Rutherford scattering by using a Legendre series expansion and assuming a continuous slowing down of the electron in the absorber. Their results are considered valid for all scattering angles and can be used with any appropriate (convergent) single-scattering cross section, for example, Mott cross section.

The evaluation of the Goudsmit-Saunders theory is discussed in detail by Berger (ref. 5) who makes use of various procedures developed by Spencer (ref. 9) that facilitate the numerical evaluation of the angular multiple-scattering distribution function. The expression developed by Berger for the intensity of electron scattering in the direction ϵ is given by

$$P_{\epsilon} = \sum_{l=0}^{\infty} (l + 1/2) \exp - \int_0^t G_l(t') dt' P_l(\cos \epsilon) \quad (6)$$

where

$$G_l(t') = 2\pi N \int_0^{\pi} \sigma(\theta, t) [1 - P_l(\cos \theta)] \sin \theta d\theta, \quad (6a)$$

N is the number of atoms per unit volume, t is the path length traversed by the electron, and $\sigma(\theta, t)$ is the single scattering cross section, whose dependence on the electron energy is expressed in the continuous slowing down approximation, through the path

length t . This expression (eq. (6)) is most applicable to a random walk procedure where the target is subdivided into equal electron energy path lengths.

Results of evaluating equation (6) are presented in table I - IV for aluminum and iron and electron energies of 0.5 and 1.0 MeV, respectively. A typical plot of multiple electron scattering is shown in figure 2 where the relative scattering probability is plotted as a function of the electron kinetic energy and angle of scattering.

Electron Backscatter Out of the Target

When a stream of electrons is directed against a solid target most of the electrons penetrate into the target; however, some return out of the incident surface again. A few of these returning electrons may be the products of collisions and are classed as secondary electrons; they are generally slow, having an energy less than 50 eV. Most of the returning electrons, however, are members of the original beam which have penetrated to a greater or lesser extent into the target, suffered elastic or inelastic collisions or both, and return to escape the surface, thus causing a reduction in the incident beam intensity.

Several authors have made measurements to determine backscattering for electrons within the energy range of interest. One such plot of electron backscattering (ref. 10) is shown in figure 3 where the ratio of backscattered to incident electrons is plotted as a function of the target atomic number and the electron kinetic energy.

Nonlinear Energy Loss of the Electron in the Target

The energy loss of electrons in a medium essentially occurs by two different mechanisms. The predominant mechanism of energy degradation at low energies is due to the inelastic collisions with the bound electrons of the medium, while at higher energies radiative collisions with the electric fields of the nuclei and the electrons become more important. It is shown in reference 11 that for lead the electron energy loss per unit path length of travel due to ionization is equal to that for radiative collisions at an approximate electron energy of 9 MeV, while for lower Z materials the equality occurs at much higher energies. Therefore, for the calculations presented herein it is assumed that the initial energy of the electron is sufficiently small so that the energy loss as a result of radiative collisions is negligible in comparison to the loss resulting from inelastic collisions.

The energy loss per cm path length (defined as stopping power) due to ionizing collisions of the electron (ref. 12) is

$$\frac{dE}{dt} = \frac{2\pi N e^4 Z}{m_0 v^2} \left[\ln \frac{m_0 v^2 E}{2I^2 (1 - \beta^2)} - \left\{ 2 \sqrt{1 - \beta^2} - 1 - \beta^2 \right\} \ln 2 + 1 - \beta^2 + \frac{1}{8} \left\{ 1 - \sqrt{1 - \beta^2} \right\}^2 \right] \quad (7)$$

where

E	total electron energy, $m_0 c^2$
N	atomic density, atms/cm^3
Z	atomic charge number
e	electron charge, 4.80288×10^{-10} , esu
\bar{I}	mean ionization potential, $m_0 c^2$
β	= v/c
m_0	electron mass, 9.1085×10^{-28} , gm
v	speed of incident electron, cm/sec
c	speed of light, 2.997929×10^{10} , cm/sec

As shown by equation (7), the energy loss per path increment is nonlinear with respect to the electron energy, for example, equal energy increments do not have corresponding path length increments and the electron loses energy at an increasing rate as it slows down. Results of evaluating equation (7) for aluminum and iron are shown in tables V and VI, respectively.

Correction for Electron-electron Bremsstrahlung

When considering the passage of an electron through a medium, one must take into account the fact that the electron may also collide with the electrons of the atoms of which the medium is composed and produce bremsstrahlung. Very laborous calculations have been made (refer to page 418 of ref. 6) to determine the exact electron-electron bremsstrahlung cross sections. These calculations

show that the final cross-section formula for electron-electron bremsstrahlung varies only slightly (except for a factor of Z^2) from the original electron-nucleus cross-section for bremsstrahlung production, although the cross-section is probably slightly smaller. This is reasonable since large momentum transfers to a single electron are, though possible, rare and contribute little to the total bremsstrahlung cross-section. The contribution to the bremsstrahlung cross-section can thus be taken into account with a reasonable degree of accuracy by replacing the Z^2 factor in the Bethe-Heitler formula (eq. (5)) by $Z(Z + 1)$.

CHAPTER IV

THE BUILDUP AND ABSORPTION OF PHOTONS IN THE TARGET

When gamma rays traverse matter, they interact through separate "elementary" processes which have the effect of attenuating the photons either by outright absorption or by degradation in energy and deflection. These predominant elementary processes are the photoelectric effect, Compton scattering and pair production.

In the photoelectric effect a photon disappears and an atomic electron leaves its atom, having absorbed the photon energy. This effect is predominant for low-energy gamma rays, especially in high Z materials.

In Compton scattering a photon is scattered inelastically and an atomic electron recoils out of an atom. This effect is predominant for 1 to 5 MeV gamma rays in high Z materials.

For pair production a gamma ray of more than 1 MeV disappears, and its energy transfers to an electron-positron pair. This effect is predominant for high gamma ray energies, especially in high Z materials.

This interaction of gamma rays with matter exhibits an exponential law of attenuation. The number of photons traveling in the original incident direction after a distance of penetration t

into the absorber is an exponentially decreasing function of the form $e^{-\mu_m t}$ where μ_m represents the mass attenuation coefficient (probability of a process per gm/cm^2).

The interaction processes experienced by photons give rise to a variety of secondary radiations, such as Compton scattered photons, electrons ejected in the photoelectric process and pair-production electrons. The decay of the photoelectric and pair-production electrons results in secondary photons which influence the whole process of photon penetration. This effect of secondary photon generation in the absorber can be taken into account by the use of the so-called buildup factor which is defined to be the ratio of the total number of gamma rays at any one point to the number of primary gamma rays. An expression (ref. 13) for the buildup factor is given by

$$B(\mu_m, t) = A_1 \exp(-a_1 \mu_m t) + A_2 \exp(-a_2 \mu_m t) \quad (8)$$

Here μ_m is the mass attenuation coefficient at the photon source energy k , and the constants A_1 , a_1 , A_2 , and a_2 are coefficients adjusted to fit experimentally determined data or theoretical data determined by Monte Carlo calculations.

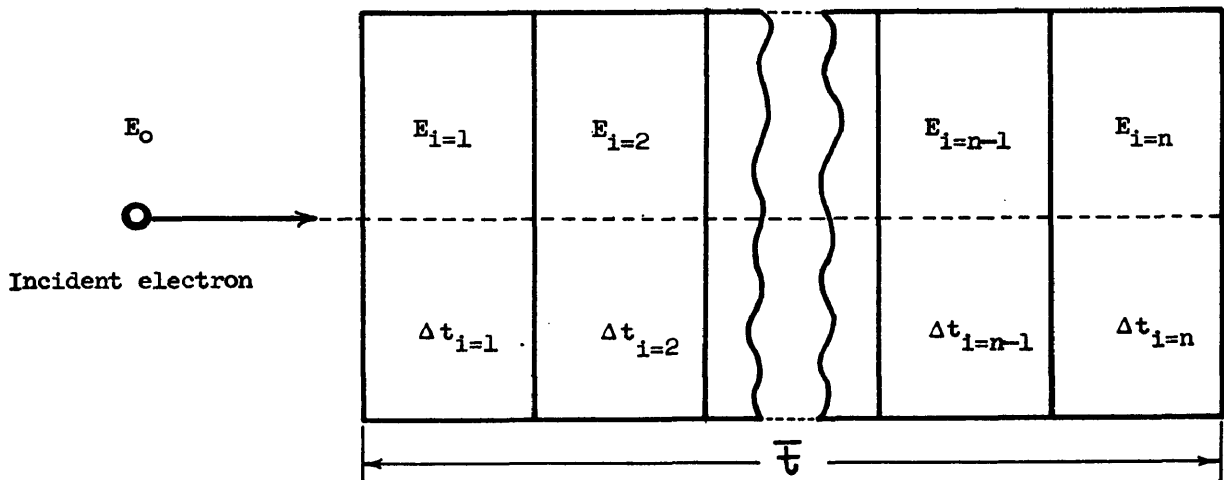
Tables VII and VIII show the attenuation and buildup coefficients μ_m , a_1 , A_1 , A_2 , and a_2 for aluminum and iron, respectively.

CHAPTER V

THE DERIVATION OF THE THICK TARGET EQUATION

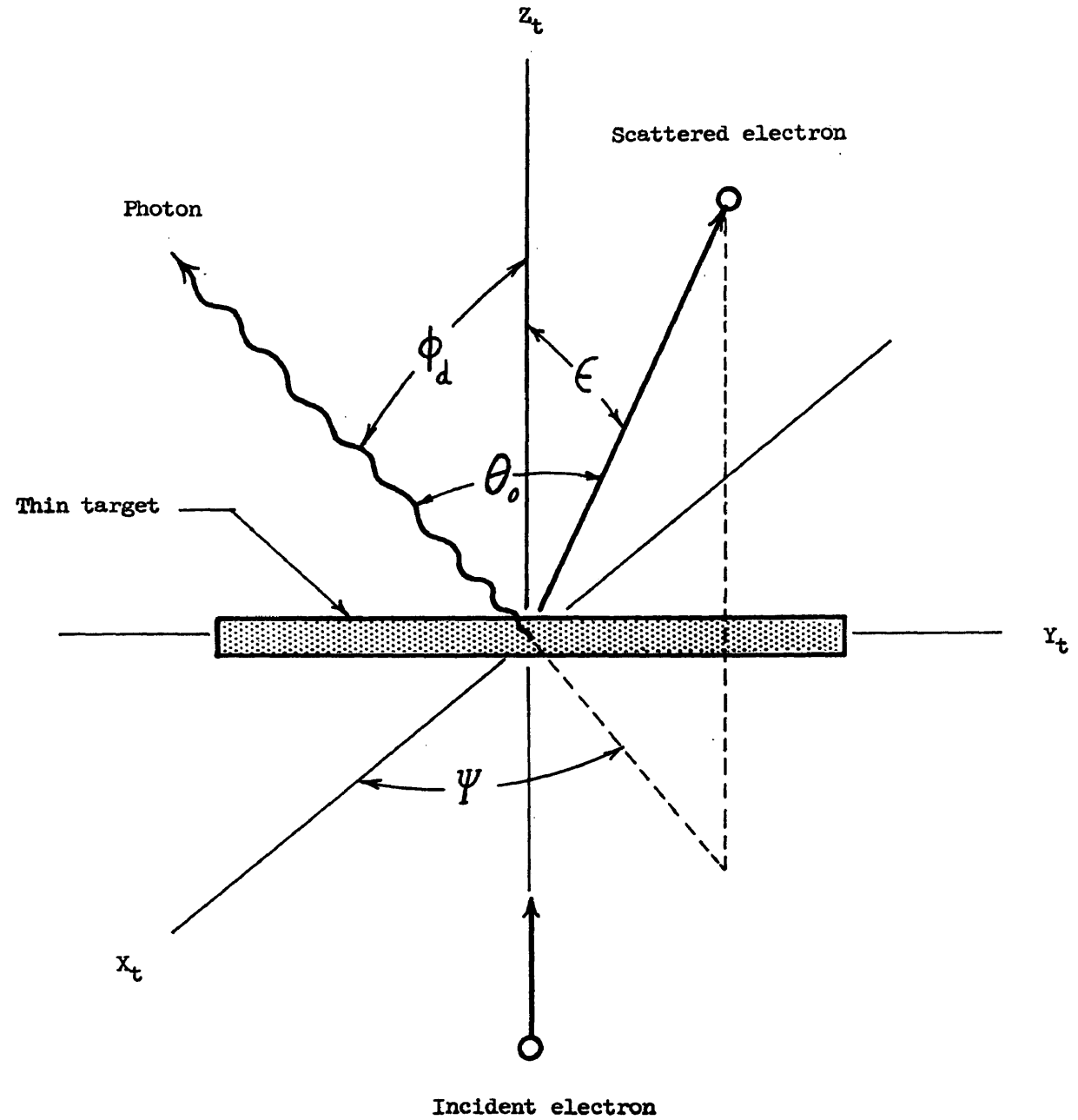
It is now possible to approximate the angular distribution of bremsstrahlung behind a thick target by the combination of the complex processes discussed in the preceding chapters.

Consider a unit monoenergetic electron flux of normal incidence on a thick target where the target has been subdivided into thin slabs or so-called thin targets as shown in sketch 5 below.



Sketch 5.- Thick target subdivision.

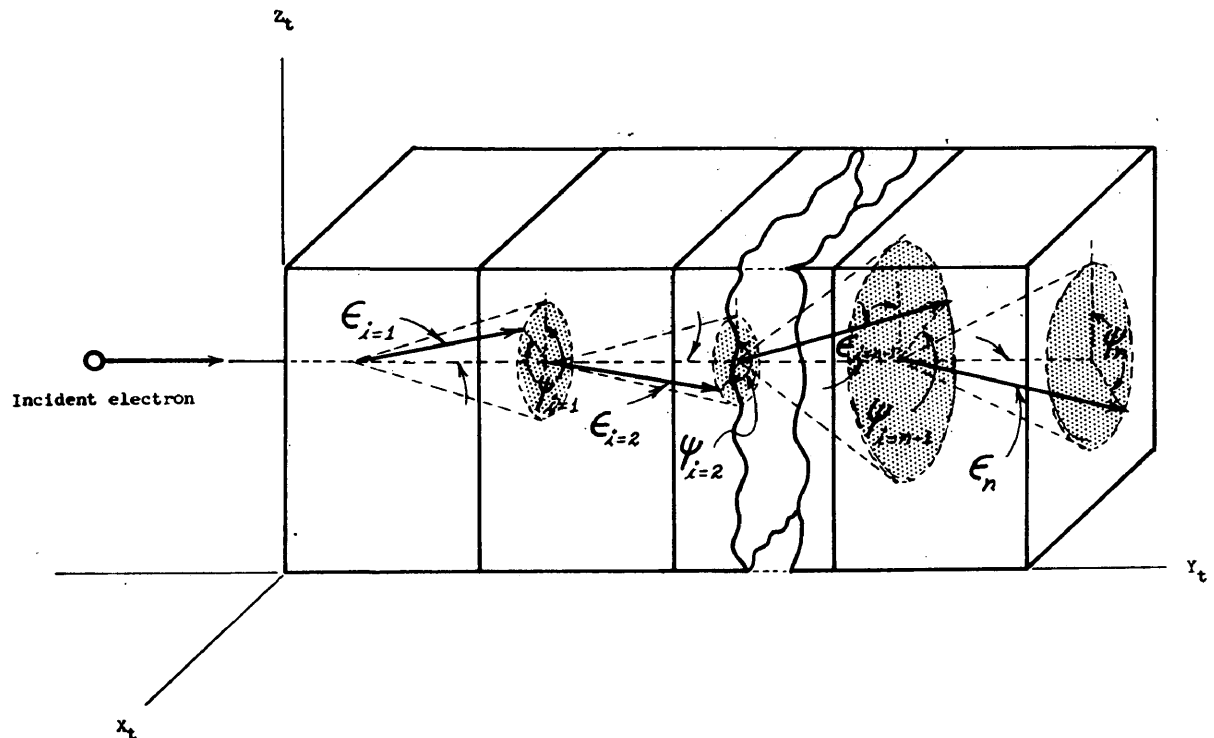
Within each thin target the incident electron will be scattered in some direction defined by the two polar angles ϵ and ψ . A schematic representation of the scattering in any slab i is shown in sketch 6. Here ϵ is the angle between the incident electron



Sketch 6.- Schematic of electron scattering
in a thin target

velocity vector and the electron direction after the electron has suffered the i th collision. Recall that the angle θ_0 is the angle between the scattered electron velocity vector and the emitted photon. Note that only photons traveling at an angle ϕ_d with respect to the incident electron direction will reach the detector.

For a thick target which consists of many thin targets there will occur a scattering, typical of the scattering shown in sketch 6, in each thin target. Sketch 7 is representative of the multiple electron scattering that occurs in a thick target. Again as in



Sketch 7.- Schematic of multiple electron scattering in a thick target.

sketch 6, ϵ and ψ are the polar angles with ϵ representing the angle between the incident electron direction and the electron velocity vector after the i th collision. Recall that the justifiable assumption is made that the lateral displacement of the electron within the target is very small compared with the distance between the target and detector and has negligible effect on the thick target spectrum. Thus the multiple scattering is considered to influence the spectrum only through changes in the electron direction with respect to the initially incident electron direction.

The path shown in sketch 7 is certainly not unique. In other words, the path of the electron in the target is random; therefore, it is necessary to consider all directions of electron scattering in each slab relative to the initial electron direction. This is to say that within each slab all possible combinations of ϵ and ψ (see sketch 6) are to be considered along with the representative probability of the electron being scattered at each particular combination of angles.

Now consider for each thin target a cylindrical differential element of volume, dV , having a normal unit area and length Δt (slab thickness) relative to the initial electron direction. The photon energy release per electron in each thin target for a specified ϵ_α , ψ_γ and ϕ_d is

$$\left[\frac{d^2 n}{dkd\Omega} (E_1, k, \theta_0) \Delta t N_l \right]_1 \quad (9)$$

where N_l is the number of atoms per cm per unit area. The photon energy release is dependent upon the angles ϵ , ψ , and ϕ_d , where these angles are related by the equation

$$\cos \theta_o = \cos \epsilon_\alpha \cos \phi_d + \sin \epsilon_\alpha \sin \phi_d \cos \psi_\gamma \quad (10)$$

Now the expression given by equation (9) is an unweighted function with respect to the electron direction, for example, the probability of the photon energy release must be multiplied by the representative probability (weighted function) of the electron being scattered at the specific values of ϵ_α and ψ_γ . This scattering probability is expressed in equation (6) which is a function of the particular thin target, electron energy, and angle ϵ as such

$$P_\epsilon = \left[P_\epsilon (E_i, \epsilon_\alpha) \right]_i \quad (11)$$

Thus for one electron direction of ϵ_α and ψ_γ the probability of the generation of a photon of energy k that will reach the detector at an angle ϕ_d is the product of the two probabilities

$$\left\{ \frac{d^2 n}{dkd\Omega} (E_i, k, \theta_o) \Delta t N_l P_\epsilon (E_i, \epsilon_\alpha) \right\}_i \quad (12)$$

For all angles of electron scattering within each slab, that is, for ϵ varying from 0 to π and ψ from 0 to 2π , the sum of the radiative probabilities in slab i is

$$\left\{ \frac{d^2 n}{dkd\Omega} \right\}_i = \sum_{\alpha=0}^{\beta} \sum_{\gamma=0}^{\delta} \left[\frac{d^2 n}{dkd\Omega} (E_1, k, \theta_0) \Delta t N_L P_{\epsilon} (E_1, \epsilon_{\alpha}) \sin \frac{\alpha\pi}{\beta} \frac{\pi}{\beta} \frac{2\pi}{\delta} \right]_i \quad (13)$$

where $\epsilon_{\alpha} = \frac{\alpha\pi}{\beta}$, $\Delta\epsilon = \frac{\pi}{\beta}$, and $\Delta\psi = \frac{2\pi}{\delta}$.

It is now necessary to sum these probabilities over the electron energy (or the corresponding thickness of the target necessary to bring the electron to rest). In theory it is possible to determine the differential path length of an electron within an absorber with the aid of equation (7), which is the relation expressing electron energy loss per cm path length. The differential path length is expressed as

$$dt = \frac{dE}{\frac{dE}{dt}} \quad (14)$$

or

$$\Delta t = \frac{\Delta E}{\frac{\Delta E}{\Delta t}} \quad (15)$$

Now substituting the above equation (15) into equation (13) and summing over i slabs in terms of the electron energy

$$\left\{ \frac{d^2 n}{dkd\Omega} \right\}_{\text{thick target}} \quad (16)$$

$$= \sum_{i=1}^n \sum_{\alpha=0}^{\beta} \sum_{\gamma=0}^{\delta} \frac{d^2 n}{dkd\Omega} (E_1, k, \theta_0) \frac{N_L}{\Delta t} P_{\epsilon} (E_1, \epsilon_{\alpha}) \sin \frac{\alpha\pi}{\beta} \frac{\pi}{\beta} \frac{2\pi}{\delta} \frac{E_0}{n}$$

where $\Delta E = E_0 n$

Now only electrons with energies greater than k can create photons of energy k , thus a lower limit is placed on the energy summation. Rewriting and regrouping equation (16) and expressing the electron energy in terms of the total electron energy we have

$$\left\{ \frac{d^2 n}{dkd\Omega} \right\} \text{thick target} \quad (17)$$

$$= N_2 \int_{k+1}^{E_0} \frac{1}{m_0 c^2} \frac{dE}{dt} \int_0^{2\pi} \int_0^\pi \left\{ \frac{d^2 n}{dkd\Omega} \right\} P_\epsilon \sin \epsilon \, d\epsilon \, d\psi \, dE$$

The additional processes of photon absorption and buildup, electron-electron bremsstrahlung and backscattering as previously discussed can now be included in equation (17),

$$\left\{ \frac{d^2 n}{dkd\Omega} \right\} \text{thick target} \quad (18)$$

$$= N_2 Z(Z+1)(1-R) \int_{k+1}^{E_0} \frac{Be^{-\mu_m t x / \cos \phi_d}}{dE/dt} \int_0^{2\pi} \int_0^\pi \frac{1}{Z^2} \frac{d^2 n}{dkd\Omega} P_\epsilon \sin \epsilon \, d\epsilon \, d\psi \, dE$$

where $e^{-\mu_m t x / \cos \phi_d}$ is the photon absorption in the target; B , the photon buildup; $Z(Z+1)$, the approximate correction for electron-electron bremsstrahlung and $(1-R)$ is the correction for electron backscattering out of the target. It is now convenient to define intensity as the photon energy k multiplied times

the number of photons $\left\{ \frac{d^2 n}{dkd\Omega} \right\}$ thick target with energy k . Thus

expressing equation (18) in terms of intensity and replacing N_z by $N_0 \rho A$.

$$\left\{ k \frac{d^2 n}{dkd\Omega} \right\} \text{ thick target} \quad (19)$$

$$= \frac{N_0}{A} Z(Z+1)(1-R) \int_{k+1}^{E_0} \frac{Be}{1} \frac{dE}{dt} e^{-\mu_m tx / \cos \phi_d} \int_0^{2\pi} \int_0^{\pi} \frac{k}{Z^2} \frac{kd^2 n}{dkd\Omega} P_\epsilon \sin \epsilon d\epsilon d\psi dE$$

where the integration

$$\int_0^{2\pi} \int_0^{\pi} P_\epsilon \sin \epsilon d\epsilon d\psi \quad (20)$$

is normalized to one in each slab. Equation (19) now represents an expression for approximating the angular distribution of bremsstrahlung behind a thick target.

CHAPTER VI

THEORETICAL RESULTS AND COMPARISONS WITH EXPERIMENTAL DATA

Because there exists a scarcity of experimental thick target data, a complete comparison between theory and experiment over a wide range of electron energies and materials cannot be made. However, experimental data do exist for aluminum and iron thick targets (ref. 14) and, where applicable, comparisons are made between theory and experiment.

The comparisons of the theoretically predicted results (eq. (19)) with the experimental data for aluminum and iron thick targets and electron kinetic energies of 0.5 and 1.0 MeV are shown in tables IX-XXIV and figures 4 and 5. Each table is representative of the thick target bremsstrahlung production for a specific material, electron kinetic energy, and detector angle. Note that the number in brackets following each entry in tables IX-XXIV indicates the power of 10 by which the entry should be multiplied.

The values presented in tables IX and XXII are plotted in figures 4 and 5 to show the general trend of comparison. Here the bremsstrahlung intensity is a function of the photon energy detector angle, electron kinetic energy, and material. The

theoretical results (obtained from evaluating eq. (19)) are seen to compare favorably with the experimental data over most of the photon energy range. The discrepancy that exists between the theoretical and experimental data is expected, inasmuch as the Born approximation technique is used in the theoretical thick target model. The reason for this discrepancy is realized by comparing experimental thin target data (ref. 14) with the Bethe-Heitler theory. Figures 6 and 7 (ref. 14) show this comparison for aluminum thin targets, detector angles of 15° and 30° , and incident electron energies of 0.5 and 1.0 MeV, respectively. It is seen from figures 6 and 7 that the Bethe-Heitler theory in general overestimates the intensity at the low photon energies and, as was previously anticipated, underestimates the spectra at the high frequency limit (i.e., upper photon energy range). In that the thick target spectra are obtained by summing up the spectra for a series of thin targets the discrepancy between the theory and experiment for the thick target is obvious and expected. Thus, the theoretical thick target results are expected to overestimate the spectrum at the low photon energies and underestimate at the high frequency limit.

It is important to try to estimate the degree of improvement of the theory, present herein, over the usual simplified approach (straight through theory) of assuming that the electron suffers

no multiple scattering. An equation describing straight through theory is

$$\left\{ \frac{k \, d^2 n}{dkd\Omega} \right\}_{\text{thick target}} = \frac{N_o \, Z^2}{A} \int_{k+1}^{E_o} \left[\frac{k \, d^2 n}{Z^2 \, dkd\Omega} \right] \frac{1}{\rho \frac{dE}{dt}} dE \quad (21)$$

One result of evaluating equation (21) for a 0.5 MeV electron incident on aluminum and with a detector angle of 30° is shown in figure 8 along with the experimental data (ref. 14) and results as predicted by equation (19). From this particular case (see fig. 8), it is obvious that the inclusion of multiple electron scattering greatly improves the method for approximating the angular distribution of thick target bremsstrahlung.

CHAPTER VII

FIRST APPROXIMATION CORRECTION TO THE THICK TARGET BREMSSTRAHLUNG SPECTRUM

The use of the Bethe-Heitler thin target cross-section in equation (19) introduces an unavoidable error in the thick target spectrum. The difficulty, as previously stated, with the thin target spectrum is that there is known to exist a discrepancy over part of the photon energy range when the theory is compared with experiment. This discrepancy was previously shown in figures 6 and 7. Also for example, the Bethe-Heitler cross-section is known to underestimate the average radiative energy release by approximately 30 percent for a single interaction of a 1.0 MeV electron in aluminum. This error increases with higher atomic numbers.

The present deficiency in the theoretical prediction of the thin target cross-section can be attributed almost entirely to the use of plane waves for the electron wave function in the matrix element as prescribed by the Born approximation. To improve the theoretical estimates, the Born approximation should be replaced with a formulation which uses electron-coulomb wave functions. Dr. C. D. Zerby (ref. NASA Contract NASw-906) is presently developing the mathematical formulation of the electron bremsstrahlung

cross-section for unpolarized incident particles using coulomb wave functions. The difficulty with the improved method, and the reason it has not been used extensively in the past, is that it does not yield a simple analytic formula, but requires extensive numerical procedures to obtain results. When Dr. Zerby's calculations are available it is presumed that the results can be tabled into the existing computer program replacing the Bethe-Heitler analytic formula.

Since no exact analytic expression exists for the thin target cross section, the next logical approach is to correct for the discrepancy in the Bethe-Heitler relation with a semiempirical or empirical correction. In the energy region of the electron rest mass energy (0.511 MeV) coulomb corrections (refer to ref. 7) to the Bethe-Heitler expression are not available in analytical form. Therefore, a correction must be approximated empirically from experimental results. The difficulty which arises is that empirical corrections cannot be determined in enough detail from the limited available experimental data to cover the entire electron energy. However, it is the belief of the author that a reasonably justifiable first approximation correction can be made to the thick target spectrum obtained by evaluating equation (19) and with the aid of thin target data presented in the same form as shown in figures 6 and 7. This correction is to be made by considering the two following important assumptions:

(a) the major contributions to the region of the intensity spectrum which is in error the most (upper region in photon energy) results from electrons with energies near the incident electron energy, that is, electrons that have just entered the incident surface, and

(b) for electron energies approximately equal to the incident electron energy the electron direction is peaked in the forward direction.

As a result of making the above two assumptions it is possible to use existing thin target experimental data to correct the thick target spectrum for some specific cases. In more general terms the thick target spectrum (obtained from eq. (19)) is to be corrected for its discrepancy with experimental results by multiplying by a correction factor defined as $\xi(k)$. This $\xi(k)$ factor is seen to be a function of the photon energy k and represents the number by which the Bethe-Heitler thin target cross-section must be multiplied so that it agrees with experimental data.

Having defined a first-approximation correction factor, the previous equation (19) can be written in the following way

$$k \frac{d^2 n}{dkd\Omega} = \frac{N_0}{A} Z(Z+1)(1-R) \int_{k+1}^{E_0} \frac{Be^{-\mu_m tx / \cos \phi_d}}{I \frac{dE}{\rho dt}} \int_0^{2\pi} \int_0^{\pi} \frac{k}{Z^2} \frac{d^2 n}{dkd\Omega} P_e \sin \epsilon d\epsilon d\psi dE$$

thick target

(22)

Now as an illustrative example, equation (22) is used to determine the bremsstrahlung spectrum for a 0.5 MeV electron incident upon an aluminum thick target with the detector angle equal to 15° . As a consequence of assumption (a) a thin target spectrum with an incident electron kinetic energy of 0.5 MeV is chosen and due to assumption (b) the angle of observation (θ_0) of the thin target spectrum is chosen to correspond with the thick target detector angle ϕ_d , that is, $\phi_d = \theta_0 = 15^\circ$. A thin target spectrum of these parameters was previously presented in figure 6 and the plot of the ξ factor for this spectrum is shown in figure 9. The results of this example are presented in figure 10 and it must be assumed that similar correction can be made to all thick target spectra provided the thin target data exist for the corresponding electron kinetic energy and observation angle.

CHAPTER VIII

CONCLUDING REMARKS

The complication of multiple electron scattering within a thick absorber prohibits a rigorous analytical solution for the prediction of the angular distribution of bremsstrahlung from completely stopped electrons. Also for electron energies that are comparable to the electron rest-mass energy no empirical formula exists for predicting thick target bremsstrahlung. Therefore, an approximating formula has been presented for predicting the thick target spectrum which is differential both in photon energy and photon angle of emittance. This formula is derived from the integration of the contributions from successive elements of thin target spectra and integrating over an energy range sufficient to bring the initial electron to rest.

The use of the thin target Born approximation cross-section for deriving the thick target expression introduces an error that is presently unavoidable. The difficulty, as previously stated, with the thin target cross-section is that it is known to be in error over part of the spectrum when comparisons are made with experiment. This discrepancy between the theory and experimental data for thin target cross-sections result in the

obvious error in the thick target spectrum. Thus it is apparent that an improved theoretical expression for thin target cross-section is needed, which would then improve the thick target results.

A first approximation correction to the thick target spectrum has been shown using experimental thin target data and considering the following assumptions:

(a) the major contribution to the region of the spectrum which is in error the most (upper region in photon energy) results from electrons with energies near the incident electron energy, and

(b) for electron energies approximately equal to the incident electron energy the electron direction is peaked in the forward direction.

The comparisons between the results obtained from the theory derived herein and experimental data are favorable and thus it can be concluded that the approximating formula for the angular distribution of electron bremsstrahlung in thick targets is valid and is an improvement over the usual straight-through theory.

INDEX OF SYMBOLS

Symbols	Definition
A	atomic weight of target material
A_1, a_1, A_2, a_2	photon buildup coefficients
B	photon buildup factor
E_i	total energy of electron emergent from thin target i (i = 1, 2,, n), in units of $m_0 c^2$
E'	total electron energy after scattering, in units of $m_0 c^2$
E_q	residual energy of scattering center after collision, in units of $m_0 c^2$
E_0	initial total electron energy, in units of $m_0 c^2$
\bar{I}	mean ionization potential, in units of $m_0 c^2$
MeV	unit of energy, million electron volts
N	atomic density, in units of atoms/cm ³
N_0	Avogadro's number, in units of atoms/gm-mole
N_z	number of atoms per cm per unit area, in units of atoms/cm ³
P_ϵ	probability of electron being scattered at an angle ϵ
P_l	Legendre polynomial
R	ratio of back-scattered electrons to primary electrons

Symbols	Definition
T	electron kinetic energy, in units of $m_0 c^2$
X_t, Y_t, Z_t	coordinate axis of target
β	number of increments in the angle ϵ
c	speed of light, in units of cm/sec
dE/dt	electron energy loss per cm path length, in units of $m_0 c^2$ -cm ² /gm
d Ω	element of solid angle in k direction, $\sin \theta_0 d\theta_0 d\phi$, in units of sr
d θ_0	element of photon angle referred to k, in units of degrees
d ϕ	element of polar angle referred to k, in units of degrees
Δt	increment in target thickness, in units of gm/cm ²
$\Delta \epsilon$	increment of polar angle ϵ of electron, in units of degrees
$\Delta \psi$	increment in polar angle ψ of electron, in units of degrees
$\Delta E, dE$	increment in total electron energy, in units of $m_0 c^2$
δ	number of increments in the angle ψ
e	electron charge, in esu units
eV	unit of energy, one electron volt
ϵ_i	polar angle of electron in thin target i, in units of degrees

Symbol	Definition
i, α, γ	indexing integers
k	vector energy of emitted photon, in units of $m_0 c^2$
$m_0 c^2$	unit of energy equal to 0.511 MeV units
m_0	electron rest mass, in units of grams
μ_m	photon mass absorption coefficient, in units of gm/cm^2
n	number of thick target subdivisions
p'	momentum vector of electron after scattering, in units $m_0 c$
p	electron momentum vector, in units of $m_0 c$
Φ_d	polar angle of detector with respect to incident electron direction, in units of degrees
π	3.1417 radians or 180°
ψ	polar angle of electron in thin target i , in units of degrees
Ω	solid angle, in units of sr
r	electron spatial displacement vector, in units of gm/cm^3
r_0	classical electron radius, $2.81784 \cdot 10^{-13}$, in units of cm
ρ	density of target material, in units of gm/cm^3
t_x	line-of-sight distance in the target material between the source point of the photon and the point at which the photon exits the back surface of the thick target, in units of gm/cm^2

Symbols	Definition
\bar{t}	mean target thickness, in units of gm/cm^2
θ_0	photon emission angle of k with respect to p_0 , in units of degrees
v	electron velocity vector after collision, in units of cm/sec
v_0	electron velocity before collision, in units of cm/sec
ξ	first approximation correction factor

REFERENCES

1. W. N. Hess, J. Geophys. Res. 68, 667-683 (1963).
2. H. A. Kramers, Phil. Mag. 46, 826 (1923).
3. R. Wilson, Proc. Phys. Soc. 66A, 638 (1953).
4. W. Wayne Scott, Electron-Bremsstrahlung Differential Cross-Sections For Thin and Thick Targets, NASA TN D-2659 (1965).
5. Martin F. Berger, Methods In Computational Physics (Academic Press, New York and London, 1963), vol. 1, pp. 135-213.
6. W. Heitler, The Quantum Theory of Radiation (Oxford University Press, London, 1954), third edition, pp. 242-256.
7. H. W. Koch and J. W. Motz, Rev. Mod. Phys. 31, 920 (1959).
8. S. Goudsmit and J. L. Saunderson, Phys. Rev. 57, 24 (1940).
9. L. V. Spencer, Phys. Rev. 98, 1507 (1955).
10. K. A. Wright and J. G. Trump, J. Appl. Phys. 33, 687, (1962).
11. Robley D. Evans, The Atomic Nucleus (McGraw-Hill Book Co., Inc., c 1955).
12. Hans A. Bethe and Julius Ashkin, Experimental Nuclear Physics (John Wiley and Sons, Inc., c 1953), vol. 1, pp. 166-357.
13. E. P. Blizzard and Lorraine S. Abbott, Reactor Handbook (Interscience Publishers, New York, 1962) vol. 3, part (b), p. 115.
14. The experimental data reported here has been supplied by Drs. L. L. Baggerly, W. E. Dance, B. J. Farmer, and J. H. Johnson of the Ling-Tempco-Vought Research Center and should be considered as preliminary data (private communications).

VITA

William Wayne Scott

Born in Chattanooga, Tennessee, May 29, 1937. Graduated from Central High School in that city, June 1956. Received his B.S. in Engineering Physics from The University of Chattanooga, January 1961; graduate student in Physics, from the University of Georgia, March 1961 through June 1962. Employed at National Aeronautics and Space Administration, Hampton, Virginia, from June 1962 to present.

In September 1963, the author entered the College of William and Mary in Virginia as a graduate student in the Department of Physics under the NASA graduate study program.

TABLE I

ANGULAR DISTRIBUTION OF MULTIPLE SCATTERED ELECTRONS IN ALUMINUM IN WHICH THE ELECTRON ENERGY IS REDUCED FROM $T_0 = 0.5$ MeV TO A VALUE T

T, MeV $\epsilon, \text{deg.}$.45	.40	.35	.30	.25	.20	.15	.10	.05
0	2.0060	1.6200	1.3500	1.0800	0.8200	0.6290	0.4520	0.3100	0.1987
15	1.5810	1.3500	1.1700	0.9580	0.7760	0.5921	0.4352	0.3001	0.1802
30	0.8200	0.7880	0.7500	0.6750	0.5984	0.4993	0.3634	0.2857	0.1920
45	0.3186	0.3510	0.3850	0.3960	0.3973	0.3703	0.3160	0.2582	0.1894
60	0.1120	0.1390	0.1700	0.2020	0.2330	0.2501	0.2271	0.2233	0.1802
75	0.0420	0.0540	0.0745	0.0980	0.1276	0.1590	0.1783	0.1860	0.1740
90	0.0189	0.0240	0.0340	0.0450	0.0683	0.0960	0.1280	0.1551	0.1561
105	0.0100	0.0120	0.0180	0.0250	0.0382	0.0553	0.0890	0.1242	0.1506
120	0.0059	0.0080	0.0100	0.0150	0.0233	0.0372	0.0627	0.1007	0.1442
135	0.0046	0.0054	0.0075	0.0100	0.0152	0.0251	0.0448	0.0830	0.1381
150	0.0036	0.0045	0.0059	0.0078	0.0110	0.0180	0.0330	0.0710	0.1383
165	0.0031	0.0038	0.0050	0.0067	0.0097	0.0155	0.0290	0.0656	0.1359
180	0.0030	0.0037	0.0049	0.0064	0.0092	0.0148	0.0279	0.0628	0.1350

TABLE II

ANGULAR DISTRIBUTION OF MULTIPLE SCATTERED ELECTRONS IN ALUMINUM IN WHICH THE ELECTRON ENERGY IS REDUCED FROM $T_0 = 1.0$ MeV TO A VALUE T

T, MeV $\epsilon, \text{deg.}$.9	.8	.7	.6	.5	.4	.3	.2	.1
0	2.4786	2.2069	1.9412	1.6831	1.4288	1.1801	0.9220	0.6613	0.4119
15	1.7000	1.6318	1.5361	1.4105	1.2564	1.0771	0.8737	0.6433	0.4087
30	0.6276	0.7210	0.8004	0.8542	0.8704	0.8382	0.7451	0.5909	0.3986
45	0.1729	0.2352	0.3133	0.4035	0.4927	0.5572	0.5735	0.5158	0.3827
60	0.0497	0.0735	0.1108	0.1661	0.2422	0.3310	0.4090	0.4286	0.3624
75	0.0179	0.0267	0.0418	0.0679	0.1129	0.1826	0.2717	0.3426	0.3395
90	0.0082	0.0120	0.0186	0.0307	0.0537	0.0983	0.1736	0.2657	0.3154
105	0.0046	0.0066	0.0099	0.0161	0.0283	0.0547	0.1098	0.2026	0.2926
120	0.0030	0.0042	0.0062	0.0098	0.0169	0.0330	0.0713	0.1545	0.2716
135	0.0022	0.0030	0.0044	0.0069	0.0115	0.0220	0.0491	0.1202	0.2539
150	0.0018	0.0025	0.0036	0.0054	0.0089	0.0165	0.0368	0.0980	0.2405
165	0.0016	0.0022	0.0031	0.0047	0.0076	0.0140	0.0308	0.0853	0.2323
180	0.0015	0.0021	0.0030	0.0045	0.0073	0.0133	0.0290	0.0817	0.2297

TABLE III

ANGULAR DISTRIBUTION OF MULTIPLE SCATTERED ELECTRONS IN IRON IN WHICH THE ELECTRON ENERGY IS REDUCED FROM $T_0 = 0.5$ MeV TO A VALUE T

T, MeV $\epsilon, \text{deg.}$.45	.40	.35	.30	.25	.20	.15	.10	.05
0	1.2476	1.1145	0.9866	0.8619	0.7264	0.5953	0.4741	0.3724	0.3221
15	1.1301	1.0324	0.9298	0.8177	0.7029	0.5818	0.4678	0.3704	0.3214
30	0.8453	0.8153	0.7696	0.7127	0.6326	0.5428	0.4495	0.3647	0.3214
45	0.5379	0.5644	0.5733	0.5635	0.5377	0.4854	0.4218	0.3564	0.3208
60	0.3051	0.3488	0.3884	0.4182	0.4299	0.4170	0.3865	0.3450	0.3202
75	0.1618	0.2021	0.2469	0.2917	0.3280	0.3474	0.3480	0.3316	0.3189
90	0.0854	0.1143	0.1518	0.1961	0.2425	0.2820	0.3089	0.3176	0.3183
105	0.0474	0.0665	0.0935	0.1304	0.1769	0.2381	0.2724	0.3042	0.3176
120	0.0289	0.0411	0.0599	0.0884	0.1294	0.1813	0.2408	0.2915	0.3164
135	0.0197	0.0279	0.0413	0.0629	0.0978	0.1483	0.2150	0.2807	0.3157
150	0.0150	0.0211	0.0313	0.0485	0.0779	0.1257	0.1961	0.2724	0.3151
165	0.0128	0.0179	0.0264	0.0411	0.0673	0.1129	0.1847	0.2673	0.3151
180	0.0121	0.0169	0.0249	0.0388	0.0638	0.1086	0.1809	0.2660	0.3144

TABLE IV
 ANGULAR DISTRIBUTION OF MULTIPLE SCATTERED ELECTRONS IN IRON IN WHICH THE ELECTRON ENERGY
 IS REDUCED FROM $T_0 = 1.0$ MeV TO A VALUE T

T, MeV $\epsilon, \text{deg.}$.9	.8	.7	.6	.5	.4	.3	.2	.1
0	1.6045	1.4244	1.2452	1.0710	0.8953	0.7227	0.5563	0.4092	0.3263
15	1.3618	1.2505	1.1275	0.9917	0.8519	0.6992	0.5451	0.4061	0.3256
30	0.8573	0.7928	0.8468	0.8032	0.7271	0.6287	0.5141	0.3965	0.3250
45	0.4286	0.4886	0.5388	0.5702	0.5697	0.5370	0.4669	0.3806	0.3237
60	0.1904	0.2451	0.3061	0.3649	0.4113	0.4301	0.4104	0.3616	0.3224
75	0.0827	0.1167	0.1625	0.2186	0.2794	0.3296	0.3508	0.3393	0.3205
90	0.0390	0.0571	0.0855	0.1274	0.1828	0.2444	0.2937	0.3158	0.3180
105	0.0207	0.0309	0.0475	0.0753	0.1188	0.1786	0.2434	0.2936	0.3160
120	0.0127	0.0187	0.0290	0.0471	0.0786	0.1310	0.2011	0.2726	0.3141
135	0.0089	0.0129	0.0197	0.0321	0.0553	0.0987	0.1695	0.2554	0.3129
150	0.0069	0.0100	0.0150	0.0243	0.0424	0.0787	0.1471	0.2427	0.3116
165	0.0069	0.0086	0.0128	0.0205	0.0358	0.0681	0.1341	0.2345	0.3110
180	0.0058	0.0082	0.0121	0.0194	0.0338	0.0646	0.1297	0.2319	0.3103

TABLE V

STOPPING POWER FOR ALUMINUM*

Atomic number(Z) = 13.00

Atomic Weight(A) = 26.9815

Electron kinetic energy MeV	Stopping power $\frac{\text{MeV} \cdot \text{cm}^2}{\text{gm}}$
0.01	0.1688E 02
.02	.1004E 02
.03	.7425E 01
.04	.6015E 01
.05	.5127E 01
.06	.4515E 01
.07	.4065E 01
.08	.3721E 01
.09	.3450E 01
.10	.3229E 01
.20	.2211E 01
.30	.1873E 01
.40	.1714E 01
.50	.1627E 01
.60	.1576E 01
.70	.1545E 01
.80	.1526E 01
.90	.1515E 01
1.00	.1509E 01
2.00	.1538E 01
3.00	.1594E 01
4.00	.1643E 01
5.00	.1685E 01
6.00	.1721E 01
7.00	.1752E 01
8.00	.1779E 01
9.00	.1804E 01
10.00	.1826E 01

*The number following the E in each tabulated entry indicates the power of 10 by which that entry should be multiplied.

TABLE VI

STOPPING POWER FOR IRON

Atomic number(Z) = 26.00

Atomic weight(A) = 55.847

Electron kinetic energy MeV	Stopping power $\frac{\text{MeV} \cdot \text{cm}^2}{\text{gm}}$
0.01	0.1452E 02
.02	.8789E 01
.03	.6546E 01
.04	.5328E 01
.05	.4556E 01
.06	.4022E 01
.07	.3629E 01
.08	.3327E 01
.09	.3089E 01
.10	.2895E 01
.20	.1996E 01
.30	.1697E 01
.40	.1557E 01
.50	.1481E 01
.60	.1437E 01
.70	.1410E 01
.80	.1395E 01
.90	.1386E 01
1.00	.1381E 01
2.00	.1416E 01
3.00	.1471E 01
4.00	.1519E 01
5.00	.1559E 01
6.00	.1594E 01
7.00	.1625E 01
8.00	.1651E 01
9.00	.1675E 01
10.00	.1697E 01

TABLE VII

ATTENUATION AND BUILDUP COEFFICIENTS FOR ALUMINUM

k, MeV	$\mu_m, \frac{\text{cm}^2}{\text{gm}}$	A1	a_1	A2	a_2
10.00E-02	1.69E-01	8.00E 00	-1.10E-01	-7.00E 00	4.40E-02
2.00E-01	1.22E-01	8.00E 00	-1.10E-01	-7.00E 00	4.40E-02
3.00E-01	1.04E-01	8.00E 00	-1.10E-01	-7.00E 00	4.40E-02
4.00E-01	9.30E-02	8.00E 00	-1.10E-01	-7.00E 00	4.40E-02
5.00E-01	8.40E-02	8.00E 00	-1.10E-01	-7.00E 00	4.40E-02
6.00E-01	7.80E-02	8.00E 00	-1.10E-01	-7.00E 00	4.40E-02
7.00E-01	7.30E-02	8.00E 00	-1.10E-01	-7.00E 00	4.40E-02
8.00E-01	6.80E-02	8.00E 00	-1.10E-01	-7.00E 00	4.40E-02
9.00E-01	6.50E-02	8.00E 00	-1.10E-01	-7.00E 00	4.40E-02
1.00E-00	6.10E-02	8.00E 00	-1.10E-01	-7.00E 00	4.40E-02
1.50E 00	5.00E-02	6.75E 00	-9.40E-02	-5.75E 00	6.90E-02
2.00E 00	4.30E-02	5.50E 00	-8.20E-02	-4.50E 00	9.30E-02
3.00E 00	3.50E-02	4.50E 00	-7.40E-02	-3.50E 00	1.16E-01
4.00E 00	3.10E-02	3.80E 00	-6.60E-02	-2.80E 00	1.30E-01
5.00E 00	2.80E-02	3.40E 00	-6.50E-02	-2.40E 00	1.41E-01
6.00E 00	2.60E-02	3.10E 00	-6.40E-02	-2.10E 00	1.52E-01
7.00E 00	2.50E-02	2.70E 00	-6.30E-02	-1.70E 00	1.50E-01
8.00E 00	2.40E-02	2.30E 00	-6.20E-02	-1.30E 00	1.50E-01
9.00E 00	2.30E-02	2.27E 00	-6.10E-02	-1.27E 00	1.39E-01
1.00E 01	2.30E-02	2.25E 00	-6.00E-02	-1.25E 00	1.28E-01

TABLE VIII

ATTENUATION AND BUILDUP COEFFICIENTS FOR IRON

k, MeV	$\mu_m, \frac{\text{cm}^2}{\text{gm}}$	A1	a_1	A2	a_2
10.00E-02	3.44E-01	1.17E 01	-9.90E-02	-1.07E 01	0.
2.00E-01	1.38E-01	1.11E 01	-9.80E-02	-1.01E 01	4.00E-03
3.00E-01	1.06E-01	1.07E 01	-9.70E-02	-9.70E 00	7.00E-03
4.00E-01	9.19E-02	1.03E 01	-9.60E-02	-9.30E 00	10.00E-03
5.00E-01	8.28E-02	1.00E 01	-9.50E-02	-9.00E 00	1.25E-02
6.00E-01	7.62E-02	9.70E 00	-9.40E-02	-8.70E 00	1.75E-02
7.00E-01	7.00E-02	9.40E 00	-9.20E-02	-8.40E 00	1.90E-02
8.00E-01	6.64E-02	9.10E 00	-9.00E-02	-8.10E 00	2.25E-02
9.00E-01	6.20E-02	8.80E 00	-8.95E-02	-7.80E 00	2.60E-02
1.00E 00	5.95E-02	8.60E 00	-8.80E-02	-7.60E 00	2.80E-02
1.50E 00	4.60E-02	7.50E 00	-8.00E-02	-6.50E 00	4.00E-02
2.00E 00	4.20E-02	6.60E 00	-7.30E-02	-5.60E 00	4.90E-02
3.00E 00	3.60E-02	5.00E 00	-7.20E-02	-4.00E 00	6.20E-02
4.00E 00	3.30E-02	4.00E 00	-7.40E-02	-3.00E 00	6.70E-02
5.00E 00	3.10E-02	3.45E 00	-7.70E-02	-2.45E 00	6.50E-02
6.00E 00	3.04E-02	3.10E 00	-8.00E-02	-2.10E 00	5.90E-02
7.00E 00	3.00E-02	2.80E 00	-8.40E-02	-1.80E 00	4.75E-02
8.00E 00	2.95E-02	2.50E 00	-8.75E-02	-1.50E 00	3.50E-02
9.00E 00	2.95E-02	2.25E 00	-9.10E-02	-1.25E 00	2.25E-02
1.00E 01	2.94E-02	2.00E 00	-9.50E-02	-1.00E 00	10.00E-03

TABLE IX

THICK TARGET BREMSSTRAHLUNG PRODUCTION

MATERIAL: Aluminum

$T_0 = 0.5$ MeV

$\phi_d = 0$ degrees

k MeV	$k \frac{d^2 n}{dkd\Omega}$ (eq. 19) $\frac{\text{MeV}}{\text{MeV-sr-electron}}$	$k \frac{d^2 n}{dkd\Omega}$ (LTV ref. 14) $\frac{\text{MeV}}{\text{MeV-sr-electron}}$
0.05	1.947 (-3)	1.450 (-3)
.10	1.426 (-3)	1.297 (-3)
.15	1.087 (-3)	1.001 (-3)
.20	8.155 (-4)	7.765 (-4)
.25	5.915 (-4)	6.348 (-4)
.30	4.029 (-4)	4.747 (-4)
.35	2.474 (-4)	3.160 (-4)
.40	1.257 (-4)	2.286 (-4)
.45	4.046 (-5)	1.056 (-4)

TABLE X

THICK TARGET BREMSSTRAHLUNG PRODUCTION

MATERIAL: Aluminum

$T_o = 0.5$ MeV

$\Phi_d = 15$ degrees

k MeV	$k \frac{d^2 n}{dkd\Omega}$ (eq. 19) MeV MeV-sr-electron	$k \frac{d^2 n}{dkd\Omega}$ (LTV ref. 14) MeV MeV-sr-electron
0.05	1.831 (-3)	1.502 (-3)
.10	1.337 (-3)	1.437 (-3)
.15	1.009 (-3)	1.080 (-3)
.20	7.579 (-4)	8.409 (-4)
.25	5.464 (-4)	6.553 (-4)
.30	3.700 (-4)	5.228 (-4)
.35	2.258 (-4)	3.816 (-4)
.40	1.141 (-4)	2.634 (-4)
.45	3.659 (-5)	1.509 (-4)

TABLE XI

THICK TARGET BREMSSTRAHLUNG PRODUCTION

MATERIAL: Aluminum

$$T_0 = 0.5 \text{ MeV}$$

$$\phi_d = 30 \text{ degrees}$$

k MeV	$k \frac{d^2 n}{dkd\Omega}$ (eq. 19) $\frac{\text{MeV}}{\text{MeV-sr-electron}}$	$k \frac{d^2 n}{dkd\Omega}$ (LTV ref. 14) $\frac{\text{MeV}}{\text{MeV-sr-electron}}$
0.05	1.482 (-3)	1.232 (-3)
.10	1.081 (-3)	1.140 (-3)
.15	8.125 (-4)	8.410 (-4)
.20	6.064 (-4)	6.453 (-4)
.25	4.336 (-4)	5.130 (-4)
.30	2.913 (-4)	3.918 (-4)
.35	1.768 (-4)	2.893 (-4)
.40	8.924 (-5)	1.969 (-4)
.45	2.884 (-5)	1.170 (-4)

TABLE XII

THICK TARGET BREMSSTRAHLUNG PRODUCTION

MATERIAL: Aluminum

$$T_0 = 0.5 \text{ MeV}$$

$$\phi_d = 60 \text{ degrees}$$

k MeV	$k \frac{d^2 n}{dkd\Omega}$ (eq. 19) $\frac{\text{MeV}}{\text{MeV-sr-electron}}$	$k \frac{d^2 n}{dkd\Omega}$ (LTV ref. 14) $\frac{\text{MeV}}{\text{MeV-sr-electron}}$
0.05	7.347 (-4)	7.691 (-4)
.10	5.252 (-4)	6.979 (-4)
.15	3.823 (-4)	4.866 (-4)
.20	2.749 (-4)	3.543 (-4)
.25	1.880 (-4)	2.642 (-4)
.30	1.211 (-4)	1.914 (-4)
.35	7.083 (-5)	1.315 (-4)
.40	3.481 (-5)	8.318 (-5)
.45	1.122 (-5)	3.964 (-5)

TABLE XIII

THICK TARGET BREMSSTRAHLUNG PRODUCTION

MATERIAL: Aluminum

$T_0 = 1.0$ MeV

$\phi_d = 0$ degrees

k MeV	$k \frac{d^2 n}{dkd\Omega}$ (eq. 19) MeV MeV-sr-electron	$k \frac{d^2 n}{dkd\Omega}$ (LTV ref. 14) MeV MeV-sr-electron
0.10	6.010 (-3)	4.986 (-3)
.20	4.367 (-3)	3.973 (-3)
.30	3.189 (-3)	3.280 (-3)
.40	2.255 (-3)	2.770 (-3)
.50	1.547 (-3)	2.286 (-3)
.70	5.773 (-4)	1.240 (-3)
.90	1.121 (-4)	3.744 (-4)

TABLE XIV

THICK TARGET BREMSSTRAHLUNG PRODUCTION

MATERIAL: Aluminum

$T_o = 1.0$ MeV

$\phi_d = 15$ degrees

k MeV	$k \frac{d^2 n}{dkd\Omega}$ (eq. 19) $\frac{\text{MeV}}{\text{MeV-sr-electron}}$	$k \frac{d^2 n}{dkd\Omega}$ (LTV ref. 14) $\frac{\text{MeV}}{\text{MeV-sr-electron}}$
0.10	5.772 (-3)	3.595 (-3)
.20	4.154 (-3)	2.861 (-3)
.30	3.001 (-3)	2.373 (-3)
.40	2.086 (-3)	2.039 (-3)
.50	1.408 (-3)	1.686 (-3)
.70	5.096 (-4)	9.395 (-4)
.90	9.412 (-5)	4.000 (-4)

TABLE XV

THICK TARGET BREMSSTRAHLUNG PRODUCTION

MATERIAL: Aluminum

$T_o = 1.0$ MeV

$\phi_d = 20$ degrees

k MeV	$k \frac{d^2 n}{dkd\Omega}$ (eq. 19) MeV MeV-sr-electron	$k \frac{d^2 n}{dkd\Omega}$ (LTV ref. 14) MeV MeV-sr-electron
0.10	5.291 (-3)	3.692 (-3)
.20	3.851 (-3)	2.756 (-3)
.30	2.772 (-3)	2.304 (-3)
.40	1.911 (-3)	1.920 (-3)
.50	1.282 (-3)	1.499 (-3)
.70	4.592 (-4)	7.970 (-4)
.90	8.426 (-5)	2.444 (-4)

TABLE XVI

THICK TARGET BREMSSTRAHLUNG PRODUCTION

MATERIAL: Aluminum

$T_0 = 1.0$ MeV

$\Phi_d = 30$ degrees

k MeV	$k \frac{d^2 n}{dkd\Omega}$ (eq. 19) $\frac{\text{MeV}}{\text{MeV-sr-electron}}$	$k \frac{d^2 n}{dkd\Omega}$ (LTV ref. 14) $\frac{\text{MeV}}{\text{MeV-sr-electron}}$
0.10	4.317 (-3)	2.502 (-3)
.20	3.076 (-3)	1.899 (-3)
.30	2.188 (-3)	1.536 (-3)
.40	1.478 (-3)	1.219 (-3)
.50	9.719 (-4)	9.329 (-4)
.70	3.377 (-4)	4.650 (-4)
.90	6.150 (-5)	1.500 (-4)

TABLE XVII

THICK TARGET BREMSSTRAHLUNG PRODUCTION

MATERIAL: Aluminum

$$T_0 = 1.0 \text{ MeV}$$

$$\Phi_d = 60 \text{ degrees}$$

k MeV	$k \frac{d^2 n}{dkd\Omega}$ (eq. 19) $\frac{\text{MeV}}{\text{MeV-sr-electron}}$	$k \frac{d^2 n}{dkd\Omega}$ (LTV ref. 14) $\frac{\text{MeV}}{\text{MeV-sr-electron}}$
0.10	1.850 (-3)	1.339 (-3)
.20	1.239 (-3)	9.464 (-4)
.30	8.028 (-4)	6.804 (-4)
.40	4.829 (-4)	5.296 (-4)
.50	2.806 (-4)	3.668 (-4)
.70	8.070 (-5)	1.410 (-4)
.90	1.358 (-5)	2.950 (-5)

TABLE XVIII

THICK TARGET BREMSSTRAHLUNG PRODUCTION

MATERIAL: Iron

$T_0 = 0.5$ MeV

$\phi_d = 0$ degrees

k MeV	$k \frac{d^2 n}{dkd\Omega}$ (eq. 19) MeV MeV-sr-electron	$k \frac{d^2 n}{dkd\Omega}$ (LTV ref. 14) MeV MeV-sr-electron
0.05	3.705 (-3)	1.282 (-3)
.10	2.676 (-3)	2.190 (-3)
.15	1.997 (-3)	1.863 (-3)
.20	1.478 (-3)	1.507 (-3)
.25	1.056 (-3)	1.249 (-3)
.30	7.101 (-4)	1.028 (-3)
.35	4.302 (-4)	7.830 (-4)
.40	2.167 (-4)	6.088 (-4)
.45	6.976 (-5)	4.296 (-4)

TABLE XIX

THICK TARGET BREMSSTRAHLUNG PRODUCTION

MATERIAL: Iron

$T_0 = 0.5$ MeV

$\phi_d = 15$ degrees

k MeV	$k \frac{d^2 n}{dkd\Omega}$ (eq. 19) MeV MeV-sr-electron	$k \frac{d^2 n}{dkd\Omega}$ (LTV ref. 14) MeV MeV-sr-electron
0.05	3.619 (-3)	4.261 (-4)
.10	2.606 (-3)	1.893 (-3)
.15	1.936 (-3)	1.592 (-3)
.20	1.426 (-3)	1.269 (-3)
.25	1.014 (-3)	1.040 (-3)
.30	6.771 (-4)	8.323 (-4)
.35	4.077 (-4)	6.494 (-4)
.40	2.039 (-4)	4.698 (-4)
.45	6.526 (-5)	3.159 (-4)

TABLE XX

THICK TARGET BREMSSTRAHLUNG PRODUCTION

MATERIAL: Iron

$$T_0 = 0.5 \text{ MeV}$$

$$\phi_d = 30 \text{ degrees}$$

k MeV	$k \frac{d^2 n}{dkd\Omega}$ (eq. 19) <u>MeV</u> MeV-sr-electron	$k \frac{d^2 n}{dkd\Omega}$ (LTV ref. 14) <u>MeV</u> MeV-sr-electron
0.05	3.281 (-3)	8.680 (-4)
.10	2.353 (-3)	1.557 (-3)
.15	1.737 (-3)	1.320 (-3)
.20	1.269 (-3)	1.052 (-3)
.25	8.953 (-4)	8.577 (-4)
.30	5.925 (-4)	6.717 (-4)
.35	3.534 (-4)	5.242 (-4)
.40	1.755 (-4)	3.698 (-4)
.45	5.595 (-5)	2.423 (-4)

TABLE XXI

THICK TARGET BREMSSTRAHLUNG PRODUCTION

MATERIAL: Iron

$T_o = 0.5$ MeV

$\Phi_d = 60$ degrees

k MeV	$k \frac{d^2 n}{dkd\Omega}$ (eq. 19) MeV MeV-sr-electron	$k \frac{d^2 n}{dkd\Omega}$ (LTV ref. 14) MeV MeV-sr-electron
0.05	2.279 (-3)	6.997 (-4)
.10	1.601 (-3)	9.952 (-4)
.15	1.143 (-3)	8.660 (-4)
.20	8.010 (-4)	6.781 (-4)
.25	5.448 (-4)	5.259 (-4)
.30	3.475 (-4)	4.008 (-4)
.35	2.001 (-4)	2.820 (-4)
.40	9.646 (-5)	1.895 (-4)
.45	3.036 (-5)	1.044 (-4)

TABLE XXII

THICK TARGET BREMSSTRAHLUNG PRODUCTION

MATERIAL: Iron

$$T_0 = 1.0 \text{ MeV}$$

$$\Phi_d = 0 \text{ degrees}$$

k MeV	$k \frac{d^2 n}{dkd\Omega}$ (eq. 19) MeV MeV-sr-electron	$k \frac{d^2 n}{dkd\Omega}$ (LTV ref. 14) MeV MeV-sr-electron
0.10	1.052 (-2)	7.318 (-3)
.20	7.592 (-3)	6.193 (-3)
.30	5.651 (-3)	5.265 (-3)
.40	4.158 (-3)	4.520 (-3)
.50	2.949 (-3)	3.769 (-3)
.70	1.178 (-3)	2.179 (-3)
.90	1.867 (-4)	8.892 (-4)

TABLE XXIII

THICK TARGET BREMSSTRAHLUNG PRODUCTION

MATERIAL: Iron

 $T_0 = 1.0$ MeV $\phi_d = 20$ degrees

k MeV	$k \frac{d^2 n}{dkd\Omega}$ (eq. 19) MeV MeV-sr-electron	$k \frac{d^2 n}{dkd\Omega}$ (LTV ref. 14) MeV MeV-sr-electron
0.10	1.004 (-2)	5.349 (-3)
.20	7.195 (-3)	4.420 (-3)
.30	5.296 (-3)	3.659 (-3)
.40	3.845 (-3)	2.941 (-3)
.50	2.681 (-3)	2.453 (-3)
.70	1.028 (-3)	1.408 (-3)
.90	1.562 (-4)	5.838 (-4)

TABLE XXIV

THICK TARGET BREMSSTRAHLUNG PRODUCTION

MATERIAL: Iron

$T_o = 1.0$ MeV

$\phi_d = 30$ degrees

<p>k</p> <p>MeV</p>	<p>$k \frac{d^2 n}{dkd\Omega}$ (eq. 19)</p> <p>$\frac{\text{MeV}}{\text{MeV-sr-electron}}$</p>	<p>$k \frac{d^2 n}{dkd\Omega}$ (LTV ref. 14)</p> <p>$\frac{\text{MeV}}{\text{MeV-sr-electron}}$</p>
0.10	8.830 (-3)	4.433 (-3)
.20	6.296 (-3)	3.589 (-3)
.30	4.600 (-3)	2.943 (-3)
.40	3.308 (-3)	2.426 (-3)
.50	2.277 (-3)	1.968 (-3)
.70	8.508 (-4)	1.217 (-3)
.90	1.278 (-4)	3.686 (-4)

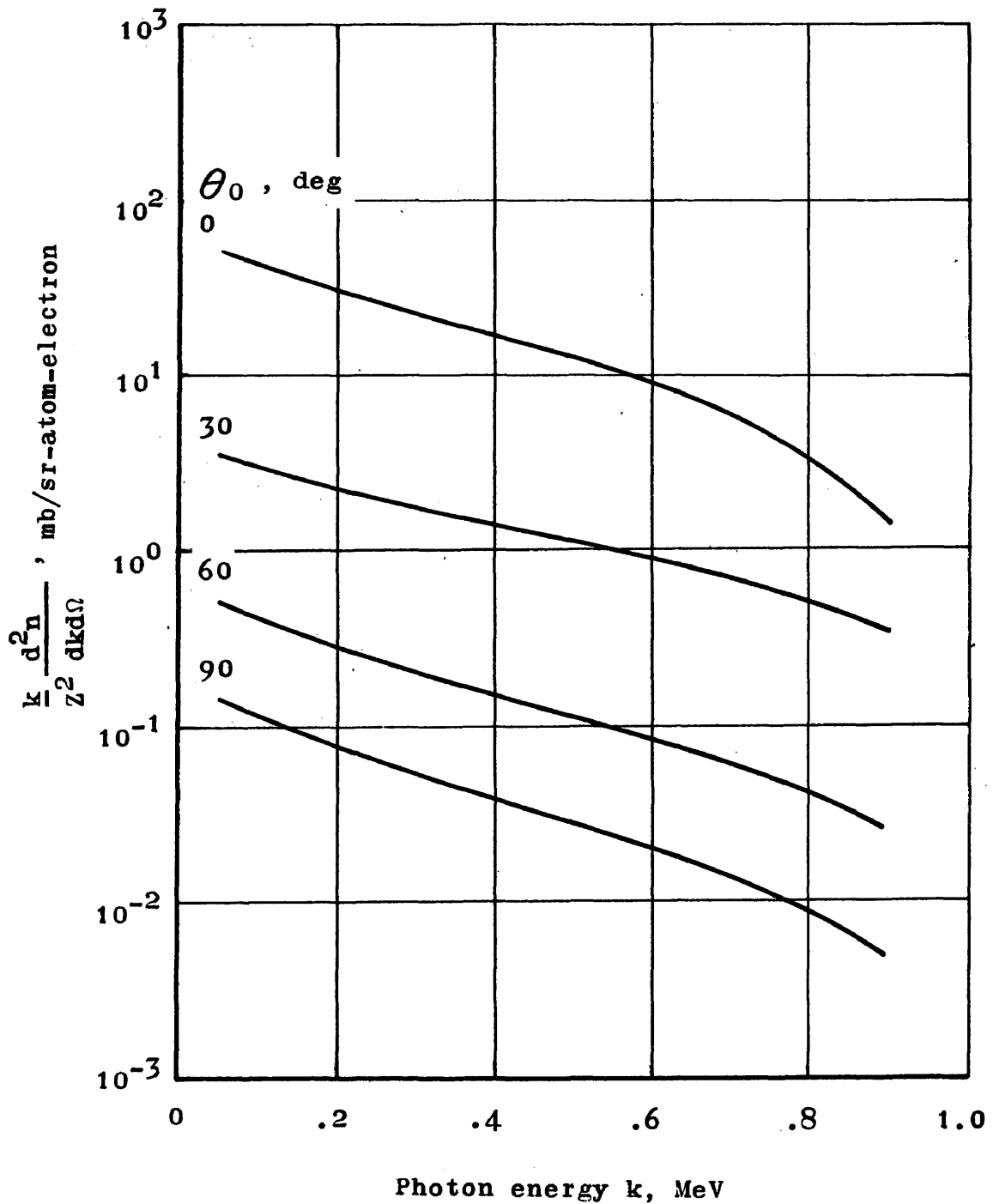


Figure 1.- Dependence of thin target bremsstrahlung intensity spectrum on photon energy k and angle θ_0 for an electron kinetic energy = 1.0 MeV.

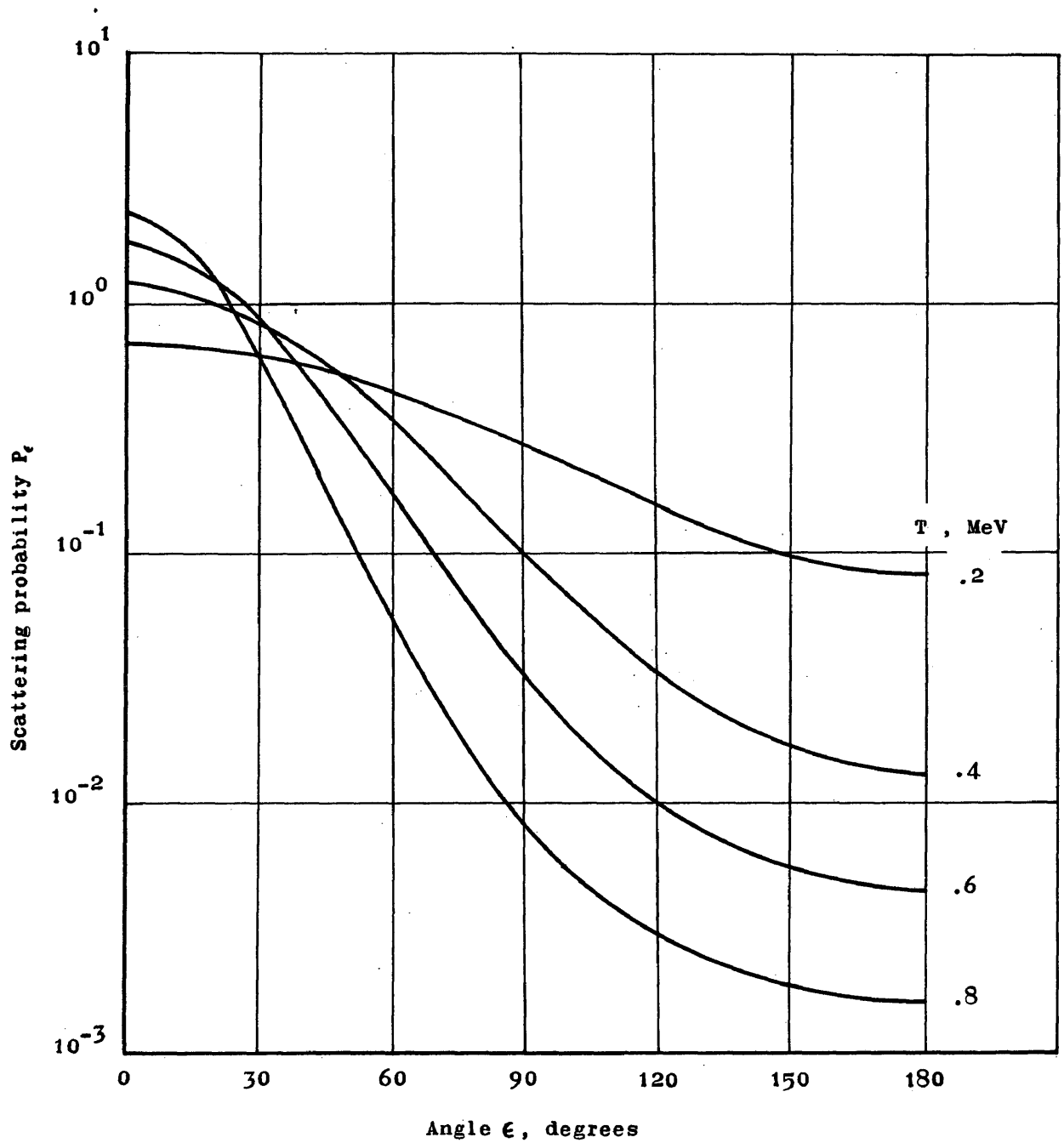


Figure 2.— Angular distribution of multiple scattered electrons in aluminum in which the electron energy is reduced from 1.0 MeV to a value T .

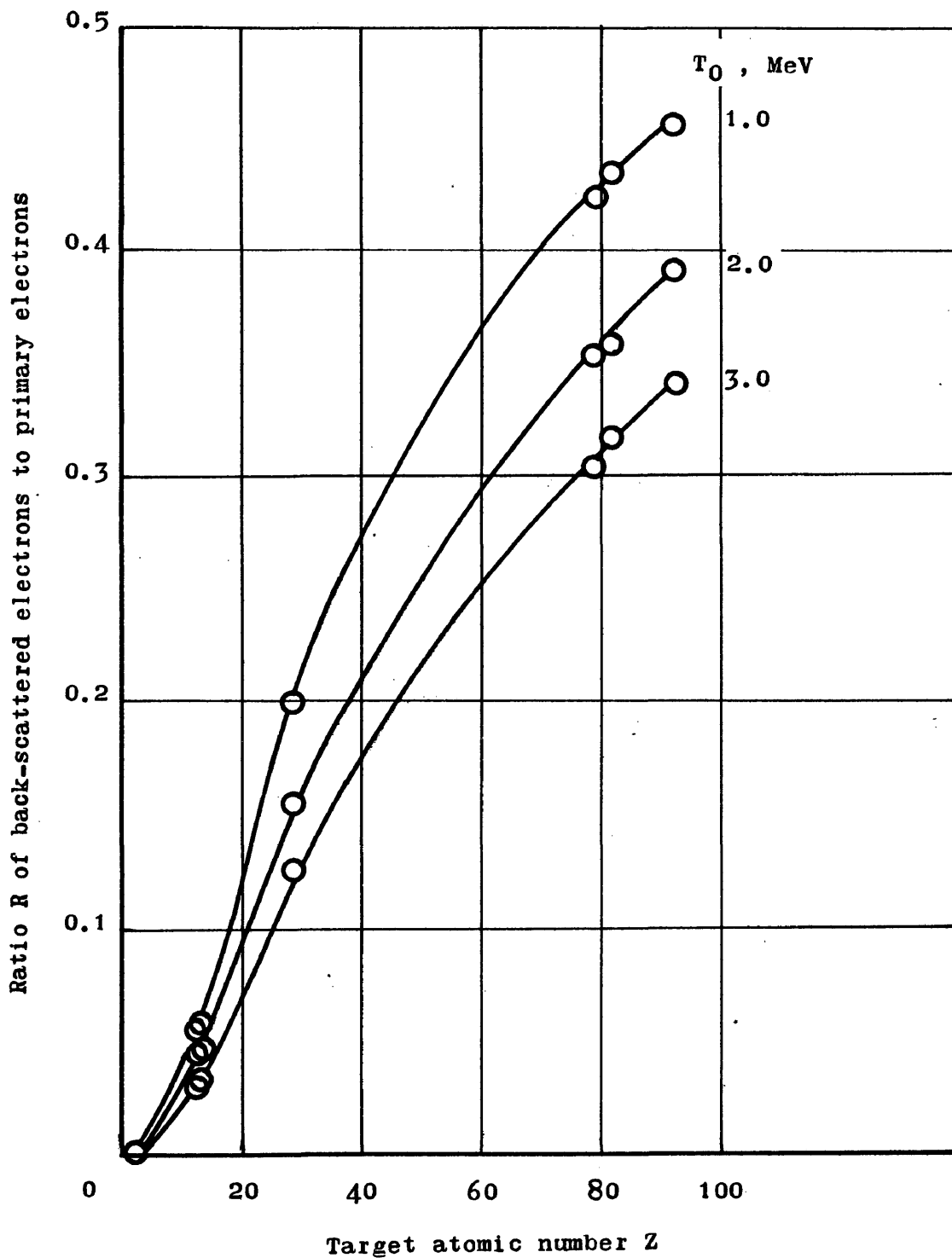


Figure 3.— Ratio of backscattered to incident megavolt electrons plotted as a function of target atomic number.

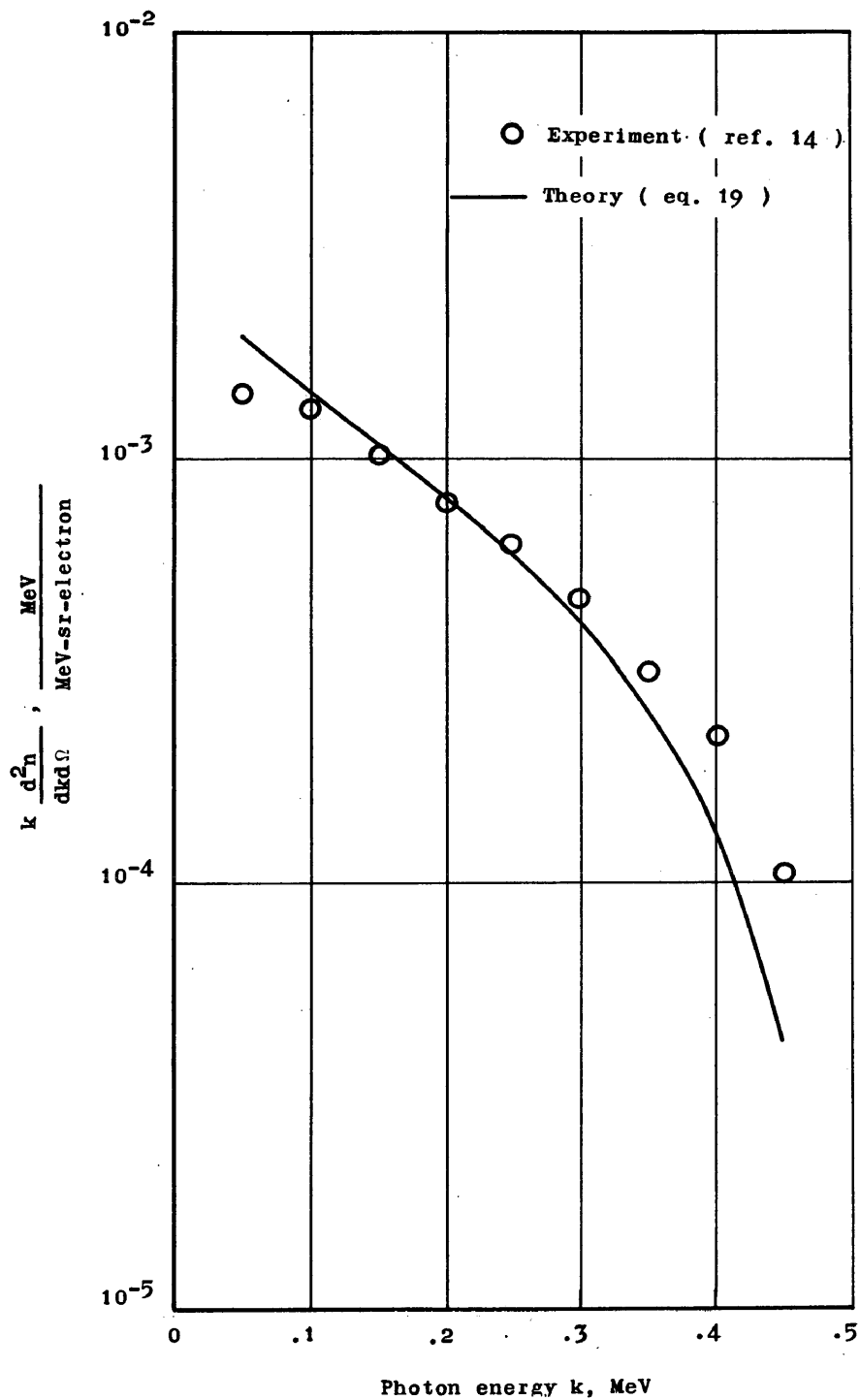


Figure 4.— Thick target bremsstrahlung production in aluminum for an incident electron kinetic energy of 0.5 MeV and a detector angle of 0°.

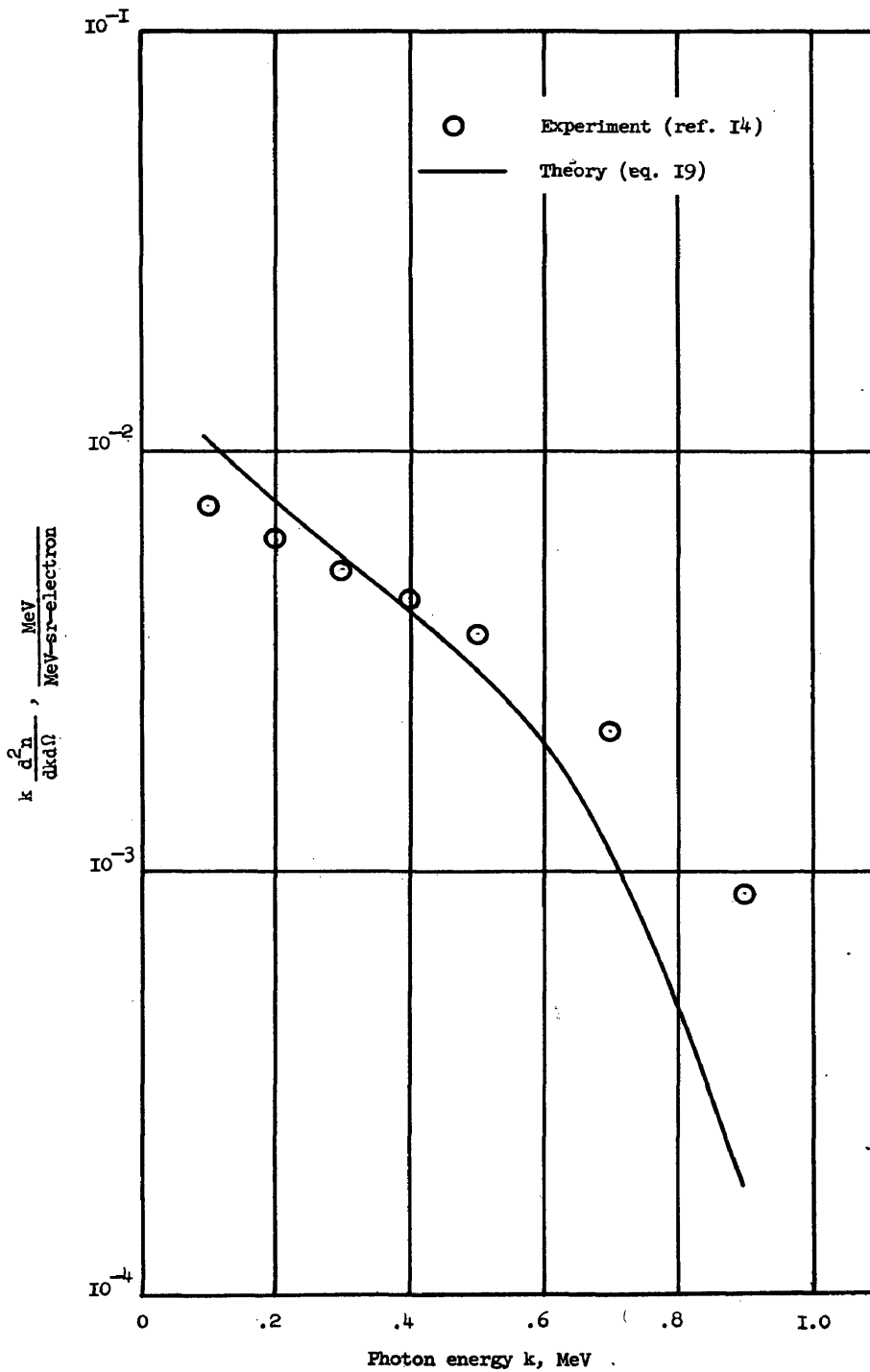


Figure 5.— Thick target bremsstrahlung production in iron for an incident electron kinetic energy of 1.0 MeV and a detector angle of 0°.

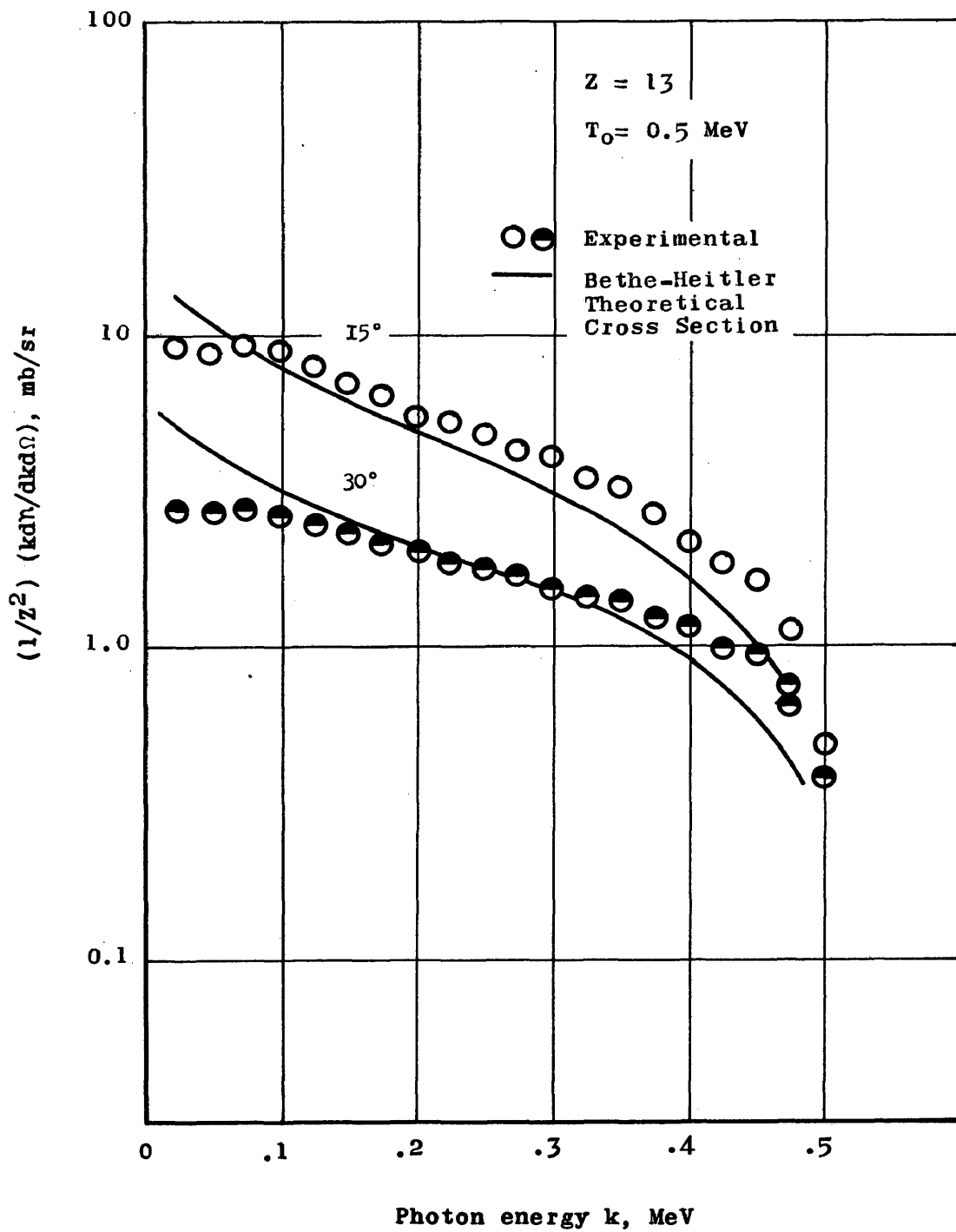


Figure 6.— Thin target differential cross sections for 0.5 MeV bremsstrahlung at photon energies k , and photon angle 15° and 30° .

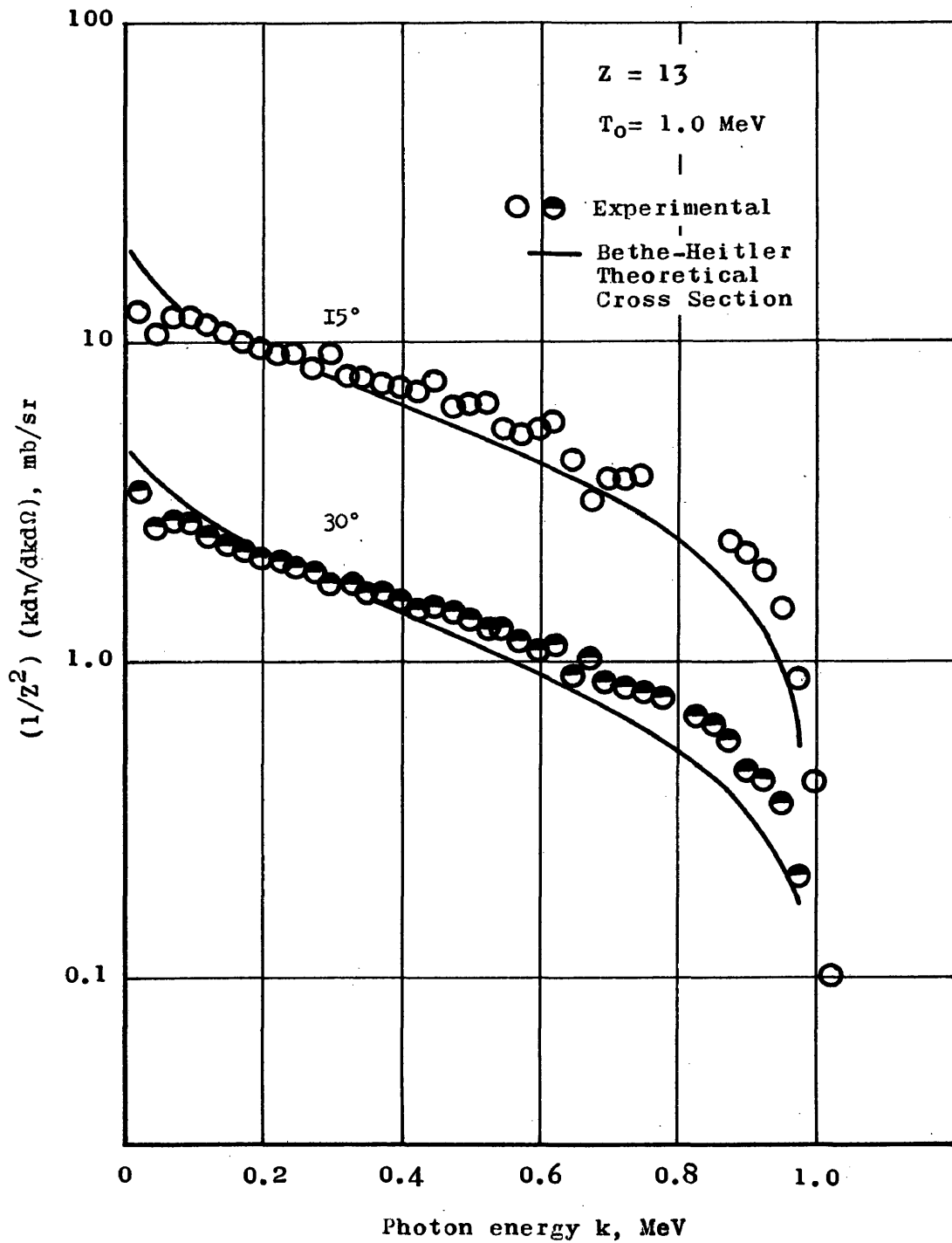


Figure 7.— Thin target differential cross sections for 1.0 MeV bremsstrahlung at photon energies k , and photon angles 15° and 30° .

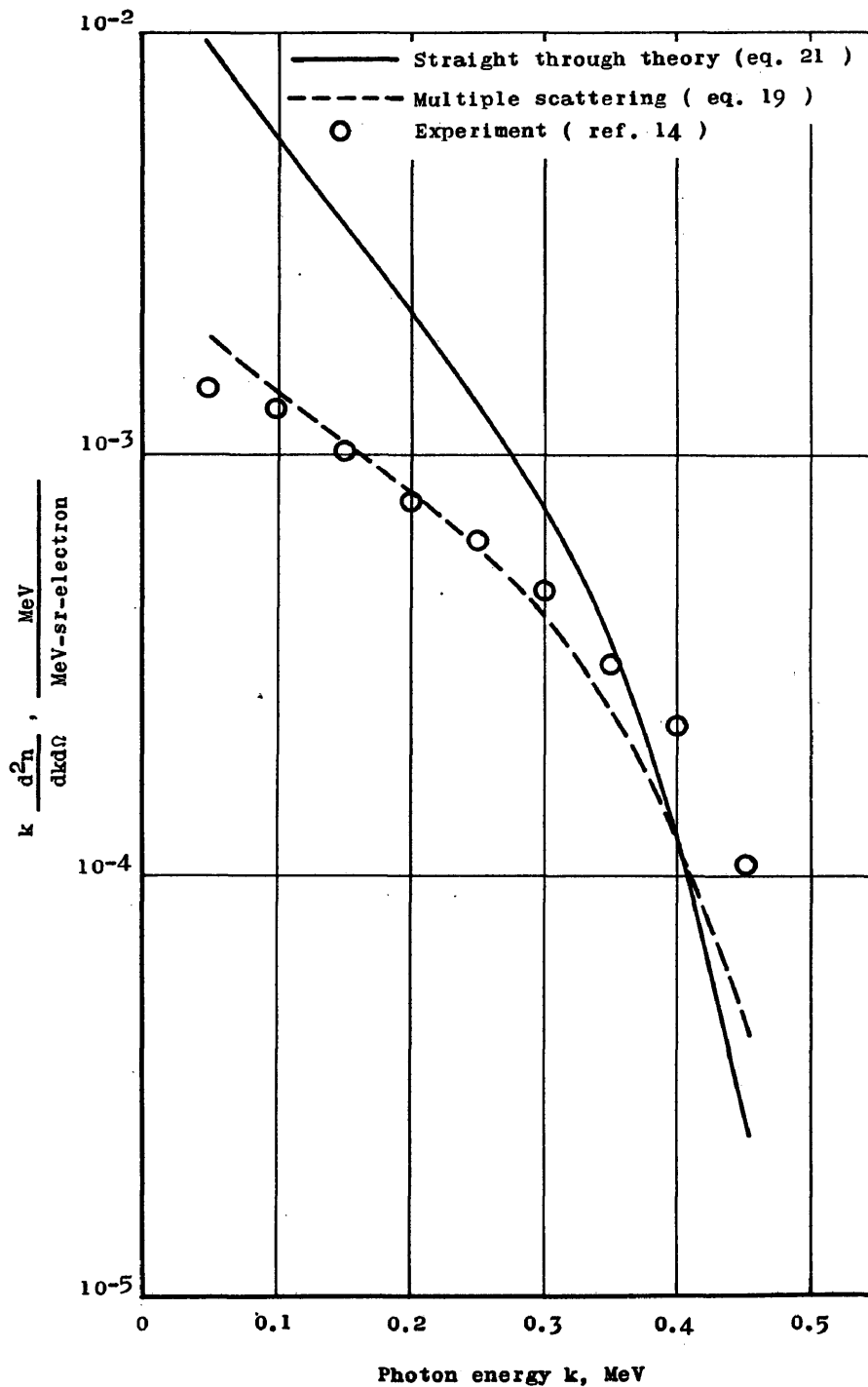


Figure 8.— Comparison of straight through theory (eq. 21) with multiple scattering theory (eq. 19) and experiment (ref. 14) for an aluminum thick target, electron kinetic energy of 0.5 MeV and detector angle of 30° .

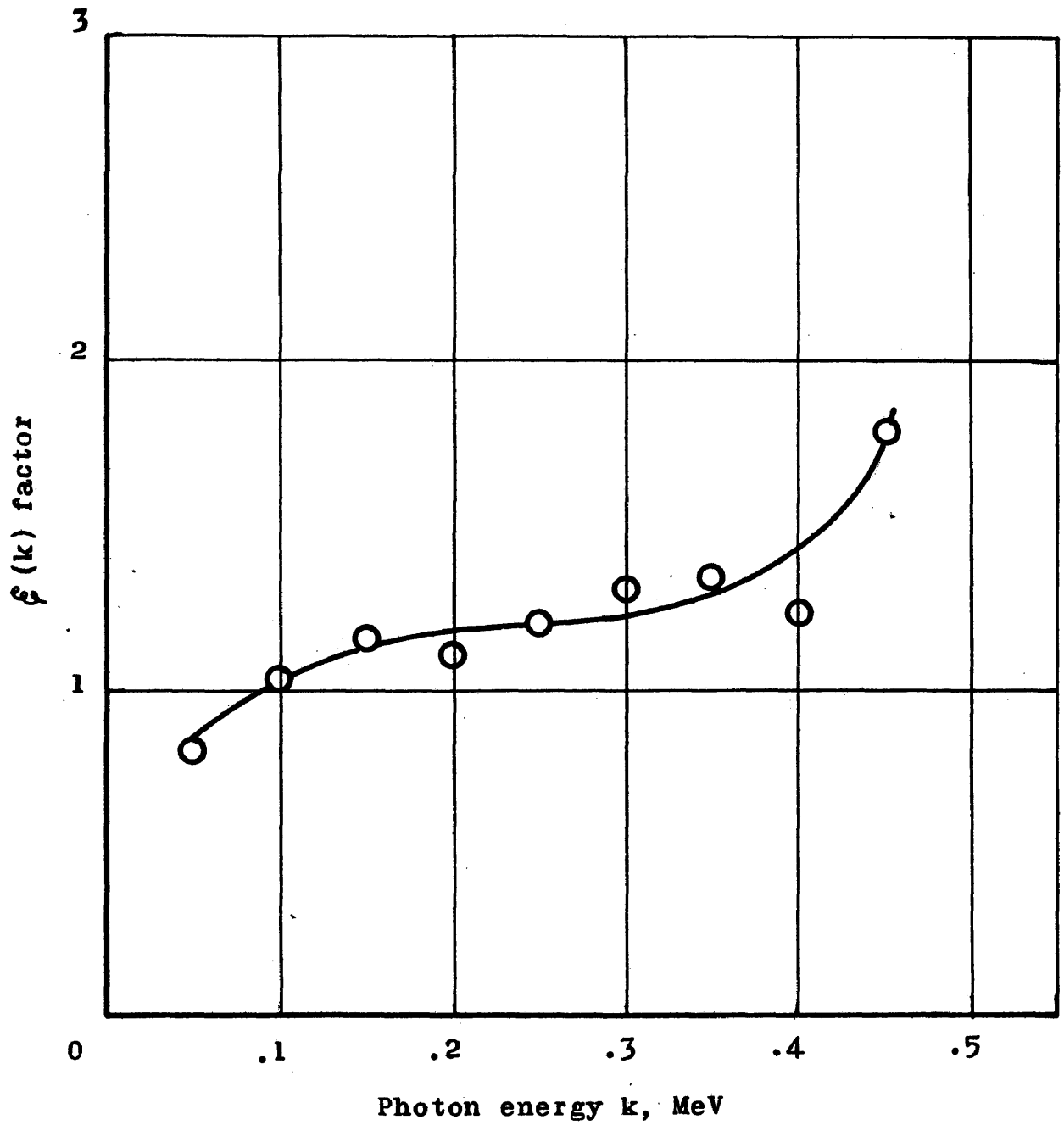


Figure 9.— A plot of the $\xi(k)$ factor for a 0.5 MeV electron incident on an aluminum target and a detector angle of 15° .

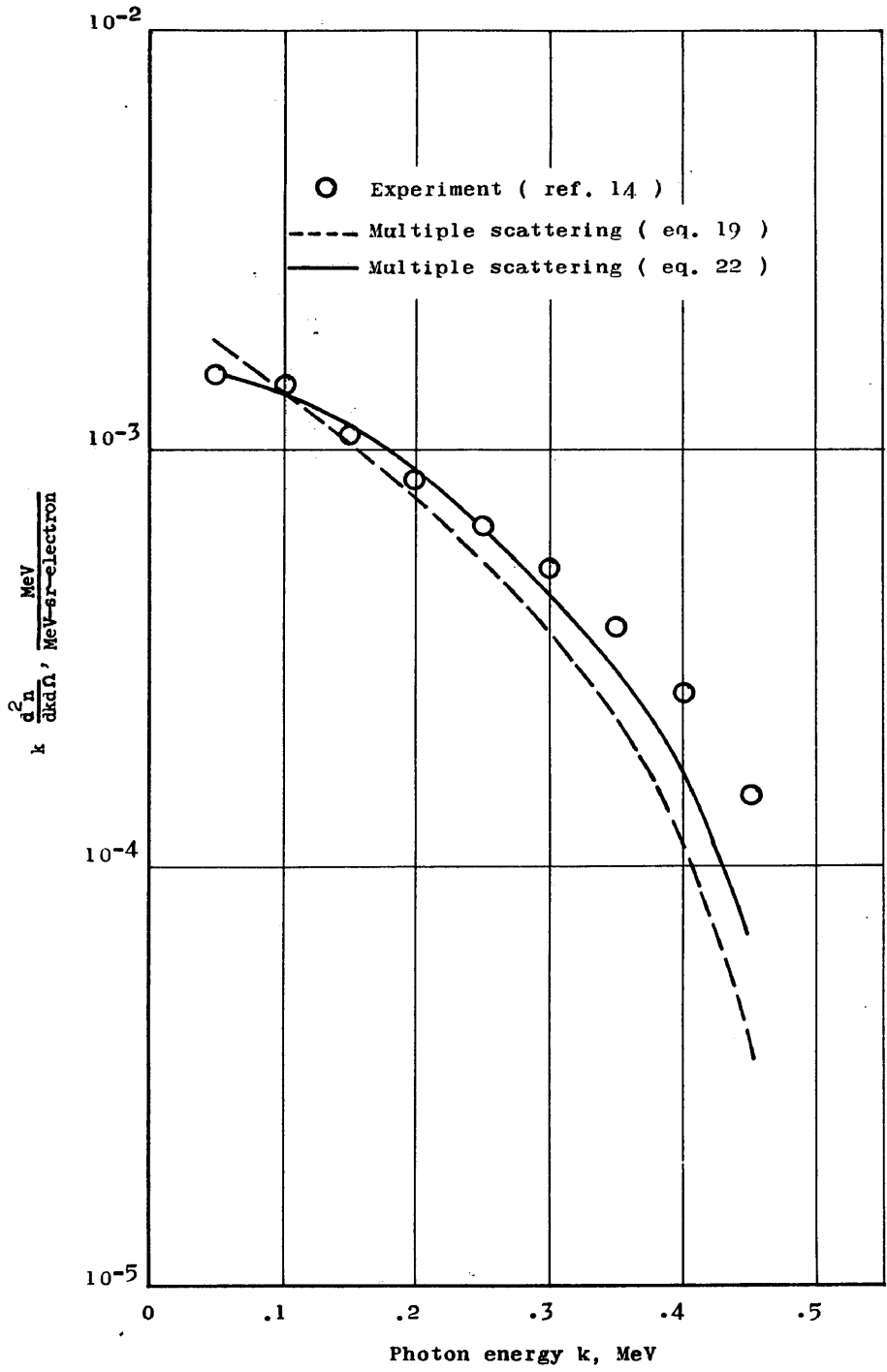


Figure 10.— Comparison of corrected multiple scattering theory (eq. 22) with multiple scattering theory (eq. 19) and experiment (ref. 14) for an aluminum thick target, electron kinetic energy of 0.5 MeV and detector angle of 15°.